

Time-dependent properties of run-and-tumble particles. I.: Density relaxation

Tanmoy Chakraborty and Punyabrata Pradhan

*Department of Physics of Complex Systems, S. N. Bose National Centre for Basic Sciences,
Block-JD, Sector-III, Salt Lake, Kolkata 700106, India*

We characterize collective diffusion of interacting run-and-tumble particles (RTPs) by explicitly calculating the bulk-diffusion coefficient $D(\rho, \gamma)$ in two minimal models on a d dimensional periodic lattice, for arbitrary density ρ and tumbling rate γ . We focus on two models: Model I is the standard version of hardcore RTPs [1], whereas model II is a long-ranged lattice gas (LLG) with hardcore exclusion - an analytically tractable variant of model I; notably, both models are found to have qualitatively similar features. In the strong-persistence limit $\gamma \rightarrow 0$ (i.e., dimensionless $r_0\gamma/v \rightarrow 0$), with v and r_0 being the self-propulsion speed and particle diameter, respectively, the fascinating interplay between persistence and interaction is quantified in terms of two length scales - mean gap, or “mean free path”, and persistence length $l_p = v/\gamma$. Indeed, for small tumbling rate, the bulk-diffusion coefficient varies as a power law in a wide range of density: $D \propto \rho^{-\alpha}$, with exponent α gradually crossing over from $\alpha = 2$ at high densities to $\alpha = 0$ at low densities. Thus, the density relaxation is governed by a nonlinear diffusion equation with anomalous spatiotemporal scaling. Moreover, in the thermodynamic limit, we show that the bulk-diffusion coefficient - for $\rho, \gamma \rightarrow 0$ with ρ/γ fixed - has a scaling form $D(\rho, \gamma) = D^{(0)}\mathcal{F}(\psi = \rho av/\gamma)$, where $a \sim r_0^{d-1}$ is particle cross-section and $D^{(0)}$ is proportional to the diffusivity of noninteracting particles; the scaling function $\mathcal{F}(\psi)$ is calculated analytically for model I and numerically for model II. Our arguments are independent of dimensions and microscopic details.

I. INTRODUCTION

Transport characteristics of self-propelled particles (SPPs), also called active matter, never cease to surprise [2]; they are often anomalous, indicating the presence of nontrivial correlations and serving as the rule rather than the exception. Numerous studies have been conducted to examine the nature of transport in SPPs - spanning from living to non-living materials (e.g., bacterial colonies and active Janus particles, respectively) - through a variety of experiments [3–13], simulations [14–16], and theories [17–20]. For instance, a recent experiment on the expansion of localized Janus swimmers on a two-dimensional substrate was found to exhibit an early-time ballistic growth [21], with the width of the density perturbation growing with time t as $\sim t^{1/z}$, characterized by the dynamic exponent $z = 1$ (ultimately crossing over to normal diffusion with $z = 2$). In a related simulation study of single-file transport of interacting SPPs, the space-time scaling of the two-point density correlations in the early-time regimes was shown to display superdiffusion with $z \approx 1.67$ [22]. Presently it is unclear precisely what causes the anomalous growth, the resultant exponent, and whether or not one should expect a universal behavior. Despite recent progress [23–29], a good theoretical understanding of the time-dependent properties of interacting SPPs, taking into consideration *many-body correlations*, is missing.

In this paper, we begin with a many-particle description of a subclass of SPPs - the hardcore run-and-tumble particles (RTPs), and provide a microscopic theory for large-scale (hydrodynamic) density relaxations in the systems. The studies of dynamical aspects of SPPs have generally been streamlined into characterizing self diffusion [19, 30–40], and other quantities such as effective

self-propulsion velocity, mechanical pressure and chemical potential, etc. [41–46], which could reveal transport-related instabilities, if any. Hardcore RTPs are possibly the simplest examples of active matter systems, with a single conserved quantity (number of particles) and average particle current that, while being persistent on smaller time scales, is exactly zero in the steady state. They provide a level playing field for theoretically investigating the time-dependent properties of such systems, which, one believes, would give a simple understanding of the fascinating aspects in more realistic active matters. In order to understand diffusive transport in an interacting-particle system such as RTPs, one must distinguish between the two transport coefficients (density-dependent in general), that characterize particle transport on large spatio-temporal scales: The self-diffusion coefficient for diffusion of individual (tagged) particles and the collective- or bulk-diffusion coefficient for spread of a density perturbation; the former determines fluctuations in the system, whereas the latter determines relaxation properties. More specifically, cumulative displacement of all particles can be related to current fluctuations [47]. The bulk-diffusion coefficient $D(\rho)$, on the other hand, is related to density relaxation, via Fick’s law for particle current,

$$J_D = -D(\rho) \frac{\partial \rho}{\partial X}, \quad (1)$$

generated due to the density gradient $\partial \rho / \partial X$.

Characterizing the bulk diffusion in interacting-particle systems is of fundamental interest in statistical physics; indeed, it is a crucial first step in formulating a fluctuating hydrodynamic formalism for diffusive systems [48, 49]. Despite significant progress made in the past [50, 51], studies to obtain the bulk-diffusion coefficient

cient exactly as a function of density (and other parameters) are rare for interacting-particle systems, particularly the conventional models of SPPs (such as hardcore RTPs), which typically have nontrivial many-body correlations. More generally, exact studies of time-dependent properties are limited to systems with a product-measure steady state [25, 52, 53], and with one [54] or two particles [24, 55, 56]. Of course, there are phenomenological theories [57, 58], however, their validity has not been rigorously proven.

Indeed, there has been some success in formulating a microscopic theoretical framework to characterize bulk diffusion and diffusive instabilities [59] in the context of active Brownian particles (ABPs). However, *exact* microscopic calculations of the bulk-diffusion coefficient, as a function of density and tumbling-rate, in *conventional* models of SPPs remain elusive. Recently, progress has been made in exactly characterizing the bulk diffusion in a specific class of RTPs, where the tumbling rate and velocity for particles are system-size dependent and vanishingly small; as a result, the system can be exactly described by a *mean-field* hydrodynamics [25]. On the contrary, for the conventional RTPs having *finite* tumbling rate and velocity, the system possesses nonzero spatial correlations (which can be even long-ranged for small tumbling rates); in that case, the hydrodynamic description of Ref. [25] is not applicable any more. In this scenario, a rigorous microscopic study of the bulk-diffusion coefficient in minimal lattice models of interacting SPPs, as considered here, are desirable.

In this paper, by using microscopic dynamical calculations, we characterize collective diffusion in hardcore run-and-tumble particles (RTPs) in d dimensions for arbitrary density ρ and tumbling rate γ , i.e., inverse of the persistence time τ_p (the persistence length being $l_p = v\tau_p$). We specifically consider two models: Model I is the standard version of hardcore RTPs introduced in [1], whereas model II is a long-ranged lattice gas (LLG), which is an analytically tractable, albeit idealized, variant of model I. We consider periodic boundary condition throughout and the total number of particles N remains conserved, with (global) density being $\rho = N/L^d$, where L is (linear) size of the system. In these two models I and II, we perform a detailed study of large-scale relaxations of the local density field $\rho(\mathbf{X}, t)$, defined at position \mathbf{X} and at time t , and relaxing from an initial density profile $\rho(\mathbf{X}, t = 0) = \rho_{in}(\mathbf{X}/L)$. We take large system-size limit $L \rightarrow \infty$, with $\rho_{in}(\mathbf{x})$ fixed, and typically consider long-wave-length fluctuations around background density ρ_0 with $\rho_{in}(\mathbf{x}) = \rho_0 + \text{const.} \sin(2\pi x)$ [i.e., $\rho(\mathbf{X}, 0) = \rho_0 + \text{const.} \sin(qX)$ with wave number $q = 2\pi/L \rightarrow 0$]. We numerically demonstrate the diffusive scaling limit of particle transport, i.e., the Fick's law as in eq. (1), through scaling collapse of density profiles at different times and for various system sizes via diffusive scaling of space and time. That is, for any finite tumbling rate and provided an initial coarse-grained profile $\rho_{in}(\mathbf{X}/L)$, the time-dependent density profile is shown to possess a dif-

fusive scaling $\rho(\mathbf{X}, t) \equiv \rho(\mathbf{x} = \mathbf{X}/L, \tau = t/L^2)$, where the evolution of the density field $\rho(\mathbf{x}, \tau)$ is governed by a nonlinear diffusion equation $\partial_\tau \rho(\mathbf{x}, \tau) = \nabla[D(\rho, \gamma)\nabla\rho(\mathbf{x}, \tau)]$, where $D(\rho, \gamma)$ is the bulk-diffusion coefficient, ρ is the density and $\gamma = \tau_p^{-1}$ is the tumbling rate. We verify the above assertion by calculating the bulk-diffusion coefficients, numerically for model I through an efficient Monte-Carlo algorithm and analytically for model II, for arbitrary density and tumbling rate in the limit of large system sizes. We then consider the special case of small density and small tumbling rate, $\rho \rightarrow 0$ and $\gamma \rightarrow 0$ with the ratio ρ/γ fixed. We show that, in the thermodynamic limit and regardless of dimensions and microscopic details, there indeed exists a scaling function $\mathcal{F}(\psi)$ governing large-scale relaxation through a precise scaling of the bulk-diffusion coefficient,

$$D(\rho, \gamma) = D^{(0)} \mathcal{F}\left(\frac{\rho av}{\gamma}\right), \quad (2)$$

where v , $a \sim r_0^{d-1}$ and r_0 are the self-propulsion speed, cross-section and diameter of particles, respectively (we throughout put $v = 1$ and $r_0 = 1$). Moreover, we analytically calculate $\mathcal{F}(\psi)$ for model II (LLG variant) and check Eq. (2) through direct simulations of both models I and II. The scaling variable $\psi = \rho v/\gamma$ quantifies the interplay between persistence and interaction, with the prefactor $D^{(0)}$ is proportional to the bulk-diffusion coefficient in the noninteracting limit. Although persistent random walks are long known in the literature [60, 61], this particular scaling function as in Eq. (2), to the best of our knowledge, has not yet been reported in the literature.

Our central idea is that collective transport in the strong-persistence limit, with $l_p \gg r_0$ - the particle diameter, is essentially governed by the two length scales, "mean free path" and persistence length. As a result, one can argue from a simple scaling theory that the bulk-diffusion coefficient has a highly nonlinear (power-law) density dependence. Interestingly, this power-law scaling of the bulk-diffusion coefficient accounts for the early-time (roughly, at the onset of diffusion) anomalous growth previously observed in Ref. [21]. Indeed we demonstrate that the early-time relaxation of initially localized density profiles are *non-Gaussian*, where their spatiotemporal scaling form, to a very good approximation, is determined within our theory. Our results suggest that the related growth exponent is *not* universal, but rather depends on specific parameter regimes.

We organize the paper in the following manner. We begin by describing two models of interacting RTPs in Sec. II, namely standard hardcore RTPs and hardcore long-range lattice gas (LLG), and present a scaling theory in Sec. III by considering the relevant length scales in both of these models. Next, we obtain the hydrodynamic description in Sec. IV by calculating the density and tumbling rate dependent bulk-diffusion coefficients $D(\rho, \gamma)$ in both models. In Sec. V A, we study the parameter dependence of the calculated $D(\rho, \gamma)$ and verify the existence

of a scaling relation in both of these models in $1D$ and $2D$. We also verify the obtained hydrodynamic description in Sec. V B by studying density relaxation obtained from numerical simulation. Next, in Sec. V C, we verify the existence of emergent hydrodynamics in both of these models in $1D$ in the limit of strong persistence. Later in , we study the relaxation of δ initial perturbation in an infinite domain to characterise early time anomalous transport. Finally, in Sec. VI, we summarise our findings with some concluding remarks.

II. MODEL DESCRIPTION

We consider two minimal models of interacting RTPs, model I and II, consisting of N particles on a d dimensional periodic hypercubic lattice with length L and volume $V = L^d$ with constant global density $\rho = N/V$. Note that, both particle diameter and lattice spacing are chosen to be equal to r_0 . While model I is the standard hardcore RTPs, model II is a “long-range” variant of model I that, as we will see, is amenable to analytical calculations. In both models, particles interact via *excluded-volume repulsion*, i.e., a site can be occupied by at most one particle and particle crossing is not allowed. We introduce the occupancy variable $\eta_{\mathbf{X}}$ at a site \mathbf{X} , where $\eta_{\mathbf{X}} = 1$ and 0 denote that the site is occupied and vacant, respectively.

Model I: Standard hardcore RTPs

We study the paradigmatic model of hardcore RTPs introduced in Ref. [1]. In this model, particles are associated with a spin variable \mathbf{s} that is randomly oriented along any of the $2d$ directions. The continuous-time stochastic dynamics of the model are as follows:

- A. *Run*: With rate v , a particle hops by unit lattice site along \mathbf{s} , provided the destination site is vacant.
- B. *Tumble*: With rate γ , a particle randomizes its spin direction, that is, it chooses a new direction at random from a set of $2d - 1$ available orientations, excluding the initial orientation direction.

It is clear from Rules A and B that, between two successive tumblings on the timescale $\tau_p = 1/\gamma$, RTPs move ballistically with constant speed v along the consecutive vacant sites in the direction of spin orientations. Also, in the noninteracting limit, the typical distance travelled by a particle on a timescale τ_p is known as *persistence length* and is defined as $l_p = v\tau_p = v/\gamma$.

Although, this model is numerically accessible, due to the extra spin variable, it is very difficult to characterize model I analytically. To overcome this difficulty, we employ an analytically tractable simpler variant of model I known as long-ranged lattice gas (LLG), which we refer to as model II below.

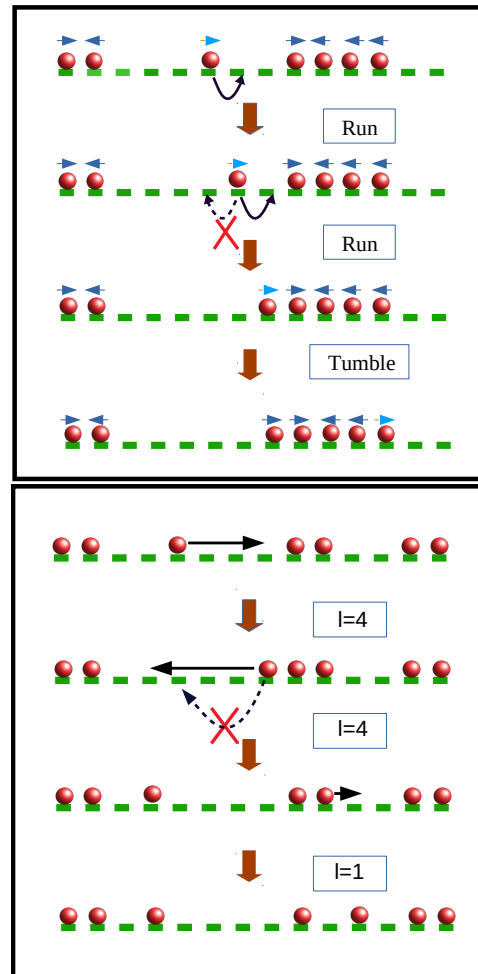


FIG. 1. *Schematic diagram of model I and II*- In the top panel, we illustrate the typical dynamics of model I (i.e., run and tumble), which is composed of standard hardcore RTPs (red circles) on a one-dimensional lattice (green rectangles). Particles to their nearest neighboring site along the associated spin indicated by the arrows above them. In the bottom panel, we demonstrate the dynamics of hardcore particles (red circle) in model II (i.e., LLG) on one dimensional lattice (green rectangle). Particles hop symmetrically by length l drawn from distribution $\phi(l) \sim e^{-l/l_p}$. The “crosses” in both panels indicate the impossibility of the time-reversed moves, as shown by the dotted arrows, and thus the violation of detailed balance at the microscopic level in both models I and II.

Model II: Hardcore long-ranged lattice gas (LLG)

We consider a long-ranged lattice gas (LLG) of N hardcore particles on a d -dimensional periodic hypercubic lattice of length L . With unit rate, a particle attempts to hop, symmetrically along any one of the $2d$ directions, by hop-length l drawn from a distribution $\phi(l)$. Provided that the stretch of consecutive vacancies from the particle along the hopping direction, called the *gap*, is at least of length l (i.e., if gap size $g \geq l$), the attempted hop is successful; otherwise, due to the hard-core constraints,

the particle traverses the entire stretch and sits adjacent to its nearest occupied site. Although the hop-length distribution $\phi(l)$ can be arbitrary, in order to compare models I and II, we choose

$$\phi(l) = B e^{-l/l_p}, \quad (3)$$

where $l_p = v/\gamma$ is the persistence length defined in model I and $B = 1 - e^{-1/l_p}$ is the normalization constant for discrete l values. Clearly, the long-ranged hopping mimics the ballistic “run” of standard RTPs, having random (exponentially distributed) “run”-lengths with a typical persistence length l_p , and is expected to capture collective behavior of model I (standard RTPs) on the persistence time-scale τ_p . Despite its simplicity, the model II (LLG) does not have a product-measure steady-state and generates nontrivial spatial correlations, resulting in clustering and large density fluctuations [62].

Although these two models have different microscopic dynamics, they have similar microscopic length scales, which we will discuss in detail in the following section.

III. RELEVANT LENGTH SCALES

Let us begin by discussing the relevant length scales in the strong persistence regime in the context of model I (it is straightforward to extend this arguments to other variants of RTPs). We do not consider thermal diffusion, being irrelevant in the strong-persistence regime. Due to persistence, particles move ballistically with a characteristic speed v (“run”) and then randomly change direction (“tumble”) with rate $\gamma = 1/\tau_p = v/l_p$ where τ_p and l_p are the persistence time and length, respectively. Clearly, l_p is a microscopic length scale induced by the persistence effect in the system. However, this persistent motion of particles is cut off by the presence of other particles along the direction of motion due to excluded-volume, or hardcore, interactions, as considered here. Consequently, there is another microscopic length-scale, induced by interaction, the mean gap $\langle g \rangle$ (equivalently, a “mean free path”) between two consecutive particles along the direction of motion. It makes no difference where the neighboring particles are (as defined by the inter-particle spacing); the physics is determined by how far, on average, the next particle is in the direction of a moving one. Indeed, l_p and $\langle g \rangle$ are the only relevant length scales in the system, carrying the signatures of persistence and interaction, respectively. Therefore, from dimensional ground, any quantities should be constructed by combining the two length scales l_p and $\langle g \rangle$. This implies that the bulk-diffusion coefficient can be cast in a form $D = D^{(0)} \mathcal{F}(l_p/\langle g \rangle)$, where scaling function $\mathcal{F}(\psi)$ depends on a *single* dimensionless scaling variable $\psi = l_p/\langle g \rangle = v/\langle g \rangle \gamma$ with the prefactor $D^{(0)} \sim \gamma l_p^2 = v^2/\gamma$. Furthermore, in the low-density limit $\rho \rightarrow 0$, as the average number of particles in any row (consisting of L sites) is equal to $L/\langle g \rangle$ and therefore

$(L/\langle g \rangle) \times (L^{d-1}/a) = N$, we obtain an exact relation,

$$\langle g \rangle = \frac{1}{\rho a}, \quad (4)$$

where $a \sim r_0^{d-1}$ and r_0 are particle cross-section and diameter, respectively. The above relation immediately leads to Eq. (2) where the scaling variable is given by $\psi = \rho a v/\gamma$ (now onwards, we put $r_0 = 1$, $a = 1$ and $v = 1$ on a hypercubic lattice of unit spacing). The asymptotic form of $\mathcal{F}(\psi)$ is determined as follows. In *noninteracting* limit $\rho \ll 1$ and $\langle g \rangle \gg l_p$, we have $D \sim l_p^2/\tau_p \sim 1/\gamma$, implying $\mathcal{F}(\psi) = \text{const.}$ as $\psi \rightarrow 0$. However, in *strongly interacting* limit $l_p \gg \langle g \rangle$, D is proportional to γ as microscopic events occur on a time scale $\tau_p = \gamma^{-1}$, implying $\mathcal{F}(\psi) \sim 1/\psi^2$ as $\psi \rightarrow \infty$. This explains the power-law dependence of D on ρ and, as we demonstrate later, the anomalous early-time relaxations. The above arguments, although plausible, must be validated, which we do next in both models I and II by obtaining their hydrodynamic descriptions.

IV. HYDRODYNAMICS

Hydrodynamics deals with large-scale spatiotemporal properties of slow variable(s). As particle number is conserved, particle density $\rho(\mathbf{X}, t) = \langle \eta_{\mathbf{X}}(t) \rangle$ is the only slow variable in the system. In that case, on a time scale much larger than the microscopic time units, density relaxation is governed by diffusive processes and, using Eq. (1) and continuity equation, we can write the time-evolution of local density,

$$\frac{\partial \rho(\mathbf{X}, t)}{\partial t} = \frac{\partial}{\partial \mathbf{X}} \cdot \left[D(\rho, \gamma) \frac{\partial \rho(\mathbf{X}, t)}{\partial \mathbf{X}} \right], \quad (5)$$

which, due to an explicit density dependence of the bulk-diffusion coefficient, is governed by a nonlinear diffusion equation and has interesting consequences. Clearly, Eq. (5) is invariant under the scale transformation $\mathbf{X} \rightarrow \lambda \mathbf{X}$ and $t \rightarrow \lambda^2 t$. Therefore, at the large space-time scale (i.e., space $\sim L$ and time $\sim L^2$), the microscopic time-evolution in Eq. (5) is reduced to the following macroscopic or hydrodynamic equation in terms of the coarse-grained space $\mathbf{x} = \mathbf{X}/L$ and time $\tau = t/L^2$:

$$\frac{\partial \rho(\mathbf{x}, \tau)}{\partial \tau} = \nabla \cdot [D(\rho, \gamma) \nabla \rho(\mathbf{x}, \tau)], \quad (6)$$

where, in this time regime, the density field $\rho(\mathbf{x} = \mathbf{X}/L, \tau = t/L^2)$ satisfies the *diffusive scaling*,

$$\rho(\mathbf{X}, t) \equiv \rho \left(\mathbf{x} = \frac{\mathbf{X}}{L}, \tau = \frac{t}{L^2} \right). \quad (7)$$

In the subsequent section, we verify the above hydrodynamic description by calculating the density and tumbling rate dependent bulk-diffusion coefficient $D(\rho, \gamma)$ for both models I and II. We develop a microscopic approach to calculate $D(\rho, \gamma)$ analytically for model II and numerically for model I.

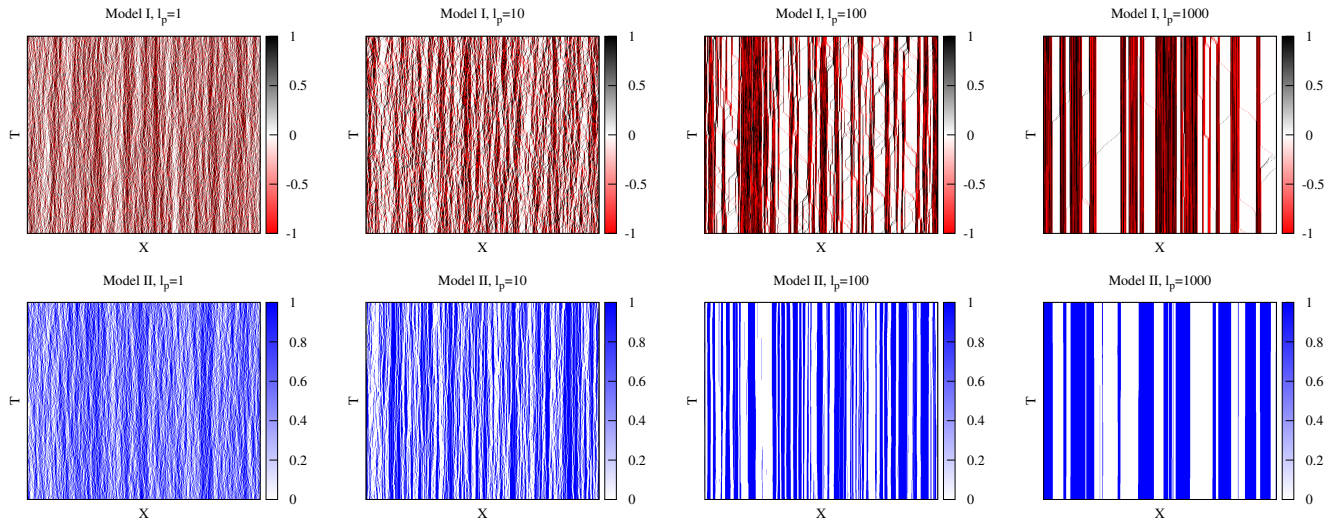


FIG. 2. *Steady-state space-time trajectory.* We plot the steady-state space-time trajectory for models I (top panel) and II (bottom panel) at the same density $\rho = 0.5$ and different persistence lengths $l_p = 1, 10, 100$, and 1000 . The black and red colors in model I represent particles with spin $s = 1$ (right mover) and $s = -1$ (left mover), respectively, while white represents the vacancy or hole. In model II, however, blue denotes particles and white denotes vacancies or holes in the system.

A. Analytical method for model II (LLG)

In this section, we describe the details of the analytical calculation scheme, which, for simplicity, are performed in one dimension, unless mentioned otherwise; in fact, generalization to higher dimensions is straightforward and the final results are given for arbitrary dimension.

An advantage of dealing with model II (LLG) is that the system possesses a *gradient property* [52], which allows the local instantaneous current to be expressed as the gradient of a local observable and the bulk-diffusion coefficient to be exactly determined in terms of the steady-state gap distribution $P(g)$. We begin our calculation by introducing the cumulative or time-integrated bond-current $Q_X(t)$, which measures the net number of particles crossing the bond $[X, X + 1]$ along the right direction in time t . It should be noted that, the stochastic variable $Q_X(t)$ is a macroscopic and experimentally measurable quantity. However, this macroscopic quantity is related to its microscopic counterpart, the instantaneous current $J_X(t)$ in the following manner:

$$J_X(t) = \lim_{\Delta t \rightarrow 0} \frac{\Delta Q_X}{\Delta t}, \quad (8)$$

where $\Delta Q_X(t) = \int_t^{t+\Delta t} J_X(t) dt$ is the time-integrated current in the time interval Δt . In this section we want to characterize its average behavior to calculate $D(\rho, \gamma)$ for model II.

Note that, whenever a particle makes long-range hop of length l and reach its destination site, it travels the entire stretch of vacant sites of that length. As a result, for a rightward (leftward) hop, current across *all* bonds in that stretch increases (decreases) by unity. Thus the continuous-time evolution for time-integrated current

$Q_X(t)$ in an infinitesimal time interval $[t, t + dt]$ can be written as

$$Q_X(t + dt) = \begin{cases} Q_X(t) + 1, & \text{prob. } \mathcal{P}_X^R(t)dt, \\ Q_X(t) - 1, & \text{prob. } \mathcal{P}_X^L(t)dt, \\ Q_X(t), & \text{prob. } 1 - (\mathcal{P}_X^R + \mathcal{P}_X^L)dt, \end{cases} \quad (9)$$

where $\mathcal{P}_X^R dt$ and $\mathcal{P}_X^L dt$ are the probabilities of the corresponding hopping events; the explicit identification of stochastic variables \mathcal{P}_X^R and \mathcal{P}_X^L are discussed below. By using the update rules, the average instantaneous current $\langle J_X(t) \rangle$ can be immediately written as

$$\langle J_X(t) \rangle = \frac{d \langle Q_X(t) \rangle}{dt} = \langle \mathcal{P}_X^R(t) \rangle - \langle \mathcal{P}_X^L(t) \rangle. \quad (10)$$

We now define the following stochastic variables, which will be required in the subsequent discussion,

$$\mathcal{U}_{X+l}^{(l)} \equiv \bar{\eta}_{X+1} \bar{\eta}_{X+2} \cdots \bar{\eta}_{X+l}, \quad (11)$$

$$\mathcal{V}_{X+l+1}^{(l+2)} \equiv \eta_X \bar{\eta}_{X+1} \bar{\eta}_{X+2} \cdots \bar{\eta}_{X+l} \eta_{X+l+1}, \quad (12)$$

where $\bar{\eta}_X = (1 - \eta_X)$, $\mathcal{U}^{(l)}$ is an indicator function of l consecutive vacant sites and $\mathcal{V}^{(l+2)}$ is that of a vacancy cluster of size l . Note that, in Eq. (9), rightward hopping events increases $Q_X(t)$ by 1, and the corresponding probability term is given by $\mathcal{P}_X^R(t)dt$. Therefore, one can identify the variable $\mathcal{P}_X^R(t)$ by simply considering the rightward hopping and computing the probability of increment in current $Q_X(t)$. Now, depending on hop-length l and gap size g , we must consider the following two possibilities:

Case I. $l > g$.— In this case, a particle crosses the entire empty stretch (cluster of vacancies) of size g during an infinitesimal time dt , and consequently the current across all g bonds is increased by unity. Therefore, for the increment in $Q_X(t)$, caused by the above hopping event, the vacancy cluster must contain the bond $(X, X+1)$ itself. However, we can keep a specific bond $(X, X+1)$ inside a hole cluster of size g by translating the entire cluster in g different ways, each of which corresponds to a unit increment of $Q_X(t)$. Therefore the probability of increment in current by unit amount is given by $\mathcal{P}_X^{>,R} dt$, where

$$\begin{aligned} \mathcal{P}_X^{>,R}(g) &\equiv \frac{1}{2} \sum_{k=1}^g \eta_{X+k-g}(t) \bar{\eta}_{X+k-g+1} \cdots \bar{\eta}_{X+k} \eta_{i+k+1}, \\ &= \frac{1}{2} \sum_{k=1}^g \mathcal{V}_{X+k+1}^{(g+2)}. \end{aligned} \quad (13)$$

Case II. $l \leq g$.— In this case, during time dt , the particle hops rightward by l units, thus increasing current by unity across all the l bonds. Consequently, $Q_X(t)$ increases by unity if the bond $(X, X+1)$ is a part of these l bonds. Similar to case I, the current $Q_X(t)$ increases by unity in l possible ways and the corresponding probability of the increment is given by $\mathcal{P}_X^{\leq,R}(t) dt$, where

$$\begin{aligned} \mathcal{P}_X^{\leq,R}(l) &\equiv \frac{1}{2} \sum_{k=1}^l \eta_{X+k-l} \bar{\eta}_{X+k-l+1} \bar{\eta}_{X+k-l+2} \cdots \bar{\eta}_{X+k}, \\ &= \frac{1}{2} \sum_{k=1}^l \left(\mathcal{U}_{X+k}^{(l)} - \mathcal{U}_{X+k}^{(l+1)} \right). \end{aligned} \quad (14)$$

Therefore, by combining cases I and II, the total probability that $Q_X(t)$ increases by unity during time interval dt , can be written as $\mathcal{P}_X^R dt$, where

$$\begin{aligned} \mathcal{P}_X^R &\equiv \sum_{l=1}^{\infty} \phi(l) \left[\mathcal{P}_X^{\leq,R}(l) + \sum_{g=1}^{l-1} \mathcal{P}_X^{>,R}(g) \right], \\ &= \frac{1}{2} \sum_{l=1}^{\infty} \phi(l) \left[\sum_{k=1}^l \left(\mathcal{U}_{X+k}^{(l)} - \mathcal{U}_{X+k}^{(l+1)} \right) + \sum_{g=1}^{l-1} \sum_{k=1}^g \mathcal{V}_{X+k+1}^{(g+2)} \right]. \end{aligned} \quad (15)$$

Similarly the total probability of current $Q_X(t)$ decreasing by unity, during time interval dt , due to leftward hopping can be written as \mathcal{P}_X^L , where

$$\mathcal{P}_X^L \equiv \frac{1}{2} \sum_{l=1}^{\infty} \phi(l) \left[\sum_{k=1}^l \left(\mathcal{U}_{X+k-1}^{(l)} - \mathcal{U}_{X+k}^{(l+1)} \right) + \sum_{g=1}^{l-1} \sum_{k=1}^g \mathcal{V}_{X+k}^{(g+2)} \right]. \quad (16)$$

By substituting $\mathcal{P}_X^R(t)$ and $\mathcal{P}_X^L(t)$ in Eq. (10), the average

instantaneous current can be immediately obtained as

$$\begin{aligned} \langle J_X(t) \rangle &= \frac{1}{2} \sum_{l=1}^{\infty} \phi(l) \left[\sum_{g=1}^{l-1} \left(\langle \mathcal{V}_{X+g+1}^{(g+2)} \rangle - \langle \mathcal{V}_{X+1}^{(g+2)} \rangle \right) \right. \\ &\quad \left. + \left(\langle \mathcal{U}_{X+l}^{(l)} \rangle - \langle \mathcal{U}_X^{(l)} \rangle \right) \right] \end{aligned} \quad (17)$$

Note that, in the above equation, $\langle J_X(t) \rangle$ is written as a (generalized) gradient of the observables $\langle \mathcal{V}^{(g+2)} \rangle$ and $\langle \mathcal{U}^{(l)} \rangle$. Now, in the large time limit, we assume that the system will reach the *local steady-state*; as a result, the variation of observables $\langle \mathcal{V}_X^{(g+2)} \rangle$ and $\langle \mathcal{U}_X^{(l)} \rangle$ depends only on the slow variable, which in this case is the local density $\rho(X, t) = \langle \eta_X(t) \rangle$ of the system. To this end, substituting $\langle \mathcal{V}_X^{(g+2)} \rangle \equiv \langle \mathcal{V}^{(g+2)} \rangle[\rho(X)]$ and $\langle \mathcal{U}_X^{(l)} \rangle \equiv \langle \mathcal{U}^{(l)} \rangle[\rho(X)]$, and performing discrete Taylor series expansion in Eq. (17), we obtain,

$$\langle J_X(t) \rangle = \frac{1}{2} \sum_{l=1}^{\infty} \phi(l) \frac{\partial}{\partial \rho} \left[\sum_{g=1}^{l-1} g \langle \mathcal{V}^{(g+2)} \rangle + l \langle \mathcal{U}^{(l)} \rangle \right] \frac{\partial \rho}{\partial X}, \quad (18)$$

Now, using the expression of $\langle J_X(t) \rangle$, the time-evolution equation of the local-density $\rho(X, t)$ can be written in the following continuity equation,

$$\begin{aligned} \frac{\partial \rho}{\partial t} &= \langle J_{X-1}(t) \rangle - \langle J_X(t) \rangle \\ &\equiv \frac{\partial}{\partial X} \left[D_{II}(\rho, \gamma) \frac{\partial \rho}{\partial X} \right], \end{aligned} \quad (19)$$

where $D_{II}(\rho, \gamma)$ is the desired bulk-diffusion coefficient for model II in one dimension, which is given by,

$$D_{II}(\rho, \gamma) = \frac{1}{2} \sum_{l=1}^{\infty} \phi(l) \frac{\partial}{\partial \rho} \left[\sum_{g=1}^{l-1} g \langle \mathcal{V}^{(g+2)} \rangle + l \langle \mathcal{U}^{(l)} \rangle \right]. \quad (21)$$

However, in arbitrary dimension d , the above expression can be written as

$$D_{II}(\rho, \gamma) = \frac{1}{2d} \sum_{l=1}^{\infty} \phi(l) \frac{\partial}{\partial \rho} \left[\sum_{g=1}^{l-1} g \langle \mathcal{V}^{(g+2)} \rangle + l \langle \mathcal{U}^{(l)} \rangle \right]. \quad (22)$$

Note that, the above equation expresses $D_{II}(\rho, \gamma)$ in terms of the correlation functions $\langle \mathcal{V}^{(g+2)} \rangle$ and $\langle \mathcal{U}^{(l)} \rangle$. Now, identifying the correlators as a function of gap distribution function $P(g)$ as,

$$\langle \mathcal{V}^{(g+2)}(\rho, \gamma) \rangle = \rho P(g), \quad (23)$$

$$\langle \mathcal{U}^{(l)}(\rho, \gamma) \rangle = \rho \sum_{g=l-1}^{\infty} (g-l+1) P(g), \quad (24)$$

(16)

we can explicitly write $D_{II}(\rho, \gamma)$ in terms of $P(g)$ as shown below,

$$D_{II}(\rho, \gamma) = -\frac{1}{2d} \frac{\partial}{\partial \rho} \left[\rho \sum_{l=1}^{\infty} \phi(l) \left(\sum_{g=1}^{l-1} gP(g) + l \sum_{g=l-1}^{\infty} (g-l+1)P(g) \right) \right]. \quad (25)$$

Of course, explicit calculation of $P(g)$ is difficult in general. However, $P(g)$ for large g is expected to be an exponential $P(g) \simeq N_* e^{-g/g_*}$, where $N_*(\rho, \gamma)$ and $g_*(\rho, \gamma)$ are the proportionality constant and typical gap size, respectively; N_* is determined from the normalization condition $\sum_g P(g) = 1$ and Eq. (4). Now, using this assumed form of $P(g)$ in Eq. (25), we obtain the following most general expression:

$$D_{II}(\rho, \gamma) = -\frac{B}{2d} \frac{\partial}{\partial \rho} \left[(1-\rho) \left\{ \frac{1}{e^{1/l_p} - 1} + \frac{1}{(e^{1/\xi} - 1)^2} \right\} \right], \quad (26)$$

where we determine the length scale as following,

$$\xi = \frac{1}{l_p^{-1} + g_*^{-1}}. \quad (27)$$

Notably, the above form of $D_{II}(\rho, \gamma)$ is valid for arbitrary ρ and γ . However, in the subsequent analysis, we consider the following special cases:

Case I: ρ arbitrary and $\gamma \rightarrow \infty$, i.e., $l_p \ll \langle g \rangle$

In this case of small persistence limit, two point density correlation vanishes. As a results, the steady-state distribution is a product measure: $P(g) \sim (1-\rho)^g \simeq e^{-g/g_*}$, where $g_* = -1/\log(1-\rho)$. Finally, using this g_* and setting the condition $\gamma \gg 1$ and ρ finite in Eq. (26), we obtain

$$D_{II}(\rho, \gamma) \simeq \frac{e^{-\gamma}}{2d} = e^{-\gamma} D_{SSEP}, \quad (28)$$

which is the bulk-diffusion coefficient $D_{SSEP} = 1/2d$ in the symmetric simple exclusion process (SSEP) up to a scale factor $exp(-\gamma)$ due to time scaling (explained below), see Appendix B for details. The exponential prefactor $e^{-\gamma}$ appears in the above equation due to the following. In this case, $\phi(l)$ has the most weight when $l = 0$, while all other hop-lengths, i.e., $l > 0$, have an exponentially lower probability $1 - \phi(0) = e^{-\gamma}$. Furthermore, among these nonzero hop-lengths $l = 1$ dominates, with contributions from larger l being negligible. As a result, in the limit $\gamma \rightarrow \infty$ or, equivalently, $l_p \rightarrow 0$ in model II (LLG), particles effectively perform SSEP-like hopping dynamics with an exponentially small rate, $e^{-\gamma}$, explaining the prefactor in Eq. (28).

Case II: $\rho \rightarrow 1$ and $\gamma \rightarrow 0$

In this regime of strong persistence and large density, persistence length l_p is much larger than the mean gap-

size $\langle g \rangle$. Although, it is easy to calculate g_* numerically in any dimensions, its analytical form is only available in one dimension [63] and is calculated to be $g_* = \sqrt{\langle g \rangle}/\gamma$, where we can straightforwardly calculate $\langle g \rangle = 1/\rho - 1$ for arbitrary density ρ (see Sec. III). Using this g_* and the condition $g_* \ll l_p \rightarrow \infty$ in Eq. (26), we obtain the following behavior of $D_{II}(\rho, \gamma)$ in this regime:

$$D_{II}(\rho, \gamma) \simeq \frac{1}{2\rho^2}, \quad (29)$$

see Appendix B for details. It is interesting to note that, in this parameter regime, $D_{II}(\rho, \gamma)$ is independent of γ and it exhibits power-law behavior with density ρ .

Case III: $\rho \rightarrow 0$ and $\gamma \rightarrow 0$

In this particular case, both of the length scales l_p and $\langle g \rangle$ are diverging as well as competing, i.e., $l_p \sim \langle g \rangle \rightarrow \infty$. Since, these two are the only relevant length scales, one may immediately construct a dimensionless quantity $\psi = l_p/\langle g \rangle$, which must be an important parameter to characterize any physical quantities in the system (see Sec III). To this end, the typical gap size should have a scaling form,

$$g_* \simeq \frac{1}{\rho} \mathcal{G}(\psi), \quad (30)$$

with $\psi = \rho v/\gamma = l_p \rho$; these assertions are verified in simulations, see Appendix A for details. The prefactor $1/\rho$ is fixed from the fact that in the limit $\psi \rightarrow 0$, the system reduces to a noninteracting one and therefore $\mathcal{G}(0) = 1$ [64]. Now, using this assumed form of g_* in Eq. (26) and putting $B = 1/l_p$, we obtain

$$D_{II}(\rho, \gamma) = \frac{e^{1/\xi}}{l_p d (e^{1/\xi} - 1)^3} \frac{1}{\mathcal{G}(\psi)} \left(1 - \psi \frac{\mathcal{G}'(\psi)}{\mathcal{G}(\psi)} \right), \quad (31)$$

where ξ is given by,

$$\xi = \frac{l_p}{1 + \psi/\mathcal{G}(\psi)}. \quad (32)$$

Furthermore, using the fact that in this limit $\xi \rightarrow \infty$, we perform the asymptotic analysis of Eq. (31), which shows $D_{II}(\rho, \gamma)$ to satisfy the following scaling relation:

$$D_{II}(\rho, \gamma)/D_{II}^{(0)} \equiv \mathcal{F}_{II}(\psi), \quad (33)$$

where $D_{II}^{(0)} = l_p^2/d$ is the diffusivity in the noninteracting limit, and $\mathcal{F}_{II}(\psi)$ is the desired scaling function, which is given by

$$\mathcal{F}_{II}(\psi) = \frac{\mathcal{G}^2(\psi)}{(\mathcal{G}(\psi) + \psi)^3} \left(1 - \psi \frac{\mathcal{G}'(\psi)}{\mathcal{G}(\psi)} \right) \quad (34)$$

see Appendix B for details.

For the purpose of illustration, we consider below the model II in one dimension. In the limit of ψ large, as shown in [63], the typical gap size in 1D is given by $g_* = \sqrt{\psi}/\rho$. Thus, combining the two limiting behaviors for small and large ψ , we have $\mathcal{G}(\psi) \simeq (1 + \psi)^{1/2}$, which is then substituted in Eq. (34) to explicitly obtain the scaling function,

$$\mathcal{F}_{II}(\psi) = \frac{(2 + \psi)}{2(\psi + \sqrt{1 + \psi})^3}. \quad (35)$$

Note that, for $\psi \ll 1$, $\mathcal{F}_{II}(\psi) = 1$ and consequently $D_{II} \simeq l_p^2$, which diverges when the persistence length $l_p \rightarrow \infty$; for $\psi \gg 1$, $\mathcal{F}_{II}(\psi) \simeq 1/2\psi^2$ and $D_{II} \simeq 1/2\rho^2$. Interestingly, expanding $\mathcal{F}_{II}(\psi)$ around $\psi = 0$, we obtain

$$\mathcal{F}_{II}(\psi) \simeq 1 - 4\psi - \mathcal{O}(\psi^2). \quad (36)$$

Now, putting back all the dimensional factors explicitly in the expression of the bulk-diffusion coefficient in Eq. (33), we get

$$D_{II}(\rho, \gamma) \simeq D_{II}^{(0)} \left(1 - \frac{\rho}{\rho_*}\right), \quad (37)$$

where we find a characteristic density $\rho_* = 1/4al_p$ and a is the particle cross-section; although the above expansion is derived in one dimension, the above form of bulk-diffusivity should be valid in any dimension with $\rho_* \sim 1/al_p$. If one assumes that the above low-density approximation ($\rho \ll \rho_*$) is valid also in the high-density regime, it would then imply that there would be a diffusive instability in the system, in the sense, for $\rho > \rho_*$, the bulk-diffusion coefficient becomes negative, i.e., $D_{II} < 0$. However, this is not the case as, in the higher density limit ($\rho \gg \rho_*$), the above expression of bulk-diffusion coefficient crosses over to a power-law and never becomes zero in the range $0 < \rho < 1$.

B. Numerical scheme for model I

According to our scaling argument, in model I (standard hardcore RTPs) too, the scaled bulk-diffusivity $D_I/D_I^{(0)} = \mathcal{F}_I(\rho v/\gamma)$ should be expressed in terms of a scaling function, which we check next. As an analytic calculation of D_I for arbitrary densities and tumbling rates is not possible at this stage, we resort to an efficient simulation technique described below [65].

In one dimension, we study the relaxation of a long wave-length (sinusoidal) initial density perturbation $\rho_{in}(X/L)$ with wave number $2\pi/L$,

$$\rho(X, 0) = \rho_0 + A(0) \sin\left(\frac{2\pi X}{L}\right), \quad (38)$$

where X is the lattice position and ρ_0 is the global density, around which the perturbation is applied. For higher

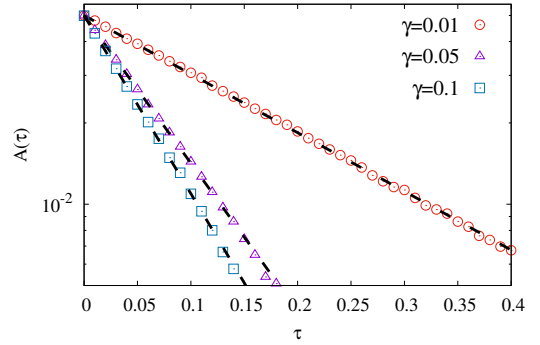


FIG. 3. Verification of Eq. (40). We plot the perturbation amplitude $A(\tau)$, as a function of the hydrodynamic time τ , for tumbling rates $\gamma = 0.01$ (red circle), 0.05 (magenta triangle) and 0.1 (blue square). The dotted black lines are the best fitted exponential functions with relaxation rates $\Gamma = 5.03$, 12.82 and 15.24 for $\gamma = 0.01$, 0.05 and 0.1 , respectively. For both these panels, we have fixed $\rho_0 = 0.5$ and $A(0) = 0.05$.

dimensions ($d > 1$), perturbation is applied in one spatial direction, while the density profile is kept uniform in all other direction. In the long-time limit $t \sim \mathcal{O}(L^2) \gg 1/\gamma$, the system is expected to forget the initial ballistic relaxations, and, as a result, on the coarse-grained scale $x = X/L$ and $\tau = t/L^2$, the density profile $\rho(x, \tau)$ evolves according to the nonlinear diffusion equation Eq. (6). In the limit of weak perturbation $A(0) \ll \rho_0$, we can simply take $D_I[\rho(x, \tau), \gamma] \simeq D_I(\rho_0, \gamma)$, and thus Eq. (6) can be written as

$$\frac{\partial \rho(x, \tau)}{\partial \tau} = D_I(\rho_0, \gamma) \frac{\partial^2 \rho(x, \tau)}{\partial x^2}. \quad (39)$$

It is worth noting that the density field $\rho(x, \tau)$ satisfies the *diffusive scaling*, as shown in Eq. (7), which we will verify shortly. Now, using Eq. (39), the density perturbation at later time can be straightforwardly calculated to have the following form: $\delta\rho(x, \tau) = \rho(x, \tau) - \rho_0 = A(\tau) \sin(2\pi x)$, with the amplitude

$$A(\tau) = A(0)e^{-\Gamma\tau}, \quad (40)$$

where Γ is the density and tumbling rate dependent the relaxation rate and is given by,

$$\Gamma(\rho_0, \gamma) = 4\pi^2 D_I(\rho_0, \gamma). \quad (41)$$

In simulations, we calculate the excess number of particles in the first half of the system $\Delta(\tau)$, which is directly related with the amplitude $A(\tau)$: $\Delta(\tau) = L^d \int_0^{1/2} \delta\rho(x, \tau) dx = L^d \pi A(\tau)$. Upon obtaining $\Delta(\tau)$ [hence $A(\tau)$] at various τ , we measure the relaxation rate and calculate the bulk-diffusion coefficient from the relation in Eq. (41). To ensure diffusive relaxation, one should first take the thermodynamic limit ($L, N \rightarrow \infty$ with $\rho_0 = N/L$ fixed) and then vary the tumbling rate γ and analyze the case of $\gamma \ll 1$. We validate

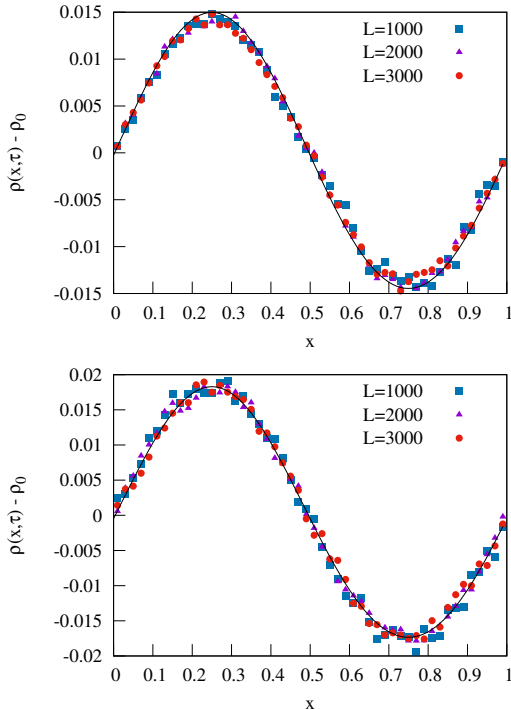


FIG. 4. *Verification of diffusive scaling.* We plot the excess density field $\delta\rho(x, \tau) = \rho(x, \tau) - \rho_0$ for $\gamma = 0.05$ (top-panel) and 0.01 (bottom-panel), obtained from simulation, as a function of the scaled position $x = X/L$ at hydrodynamic times $\tau = 0.1$ and 0.2 , respectively. We relax the system with a sinusoidal initial condition defined in Eq. (38) with $\rho_0 = 0.5$ and $A(0) = 0.05$. Corresponding lines are obtained by numerically integrating the hydrodynamic equation Eq. (6) using the obtained bulk-diffusion coefficients.

Eq. (40) in one dimension by plotting the numerically obtained $A(\tau)$ as a function of τ for various tumbling rates $\gamma = 0.01, 0.05$, and 0.1 at density $\rho_0 = 0.5$ and system size $L = 1000$. Indeed, we find $A(\tau)$ to be exponential, as predicted by Eq. (40). Fitting the obtained simulation data with Eq. (40) yields the corresponding relaxation rates Γ , which then using in Eq. (41), we finally obtain the bulk-diffusion coefficient for model I at the corresponding parameter values.

Numerical verification of diffusive scaling

One of the central assumptions in calculating $D_I(\rho, \gamma)$ in preceding section is the existence of diffusive scaling limits as expressed in Eqs. (6) and (7). We can immediately verify, through direct Monte Carlo simulations, the existence of such a diffusive scaling limit for model I (standard hardcore RTPs), which also leads to a direct verification of Eqs. (6) and (7). To this end, we study the relaxation of (hydrodynamic) density field $\rho(x, \tau)$ as a function of scaled position $x = X/L$ for different system sizes L and different microscopic times $t \sim \mathcal{O}(L^2)$ such

that the hydrodynamic time $\tau = t/L^2$ remains fixed. The scaling limit would be verified if different curves corresponding to different L at the same hydrodynamic time τ collapse onto each other and, in that case, the collapsed data must be the solution of the nonlinear diffusion equation as given in Eq. (6).

To implement the above numerical scheme, we simulate model I (for simplicity, in one dimension) with the initial sinusoidal density profile, as defined in Eq. (38), with background $\rho_0 = 0.5$ and perturbation height $A(0) = 0.05$. In Fig. IV B, we plot the numerically obtained excess density field $\delta\rho(x, \tau) = \rho(x, \tau) - \rho_0$ for tumbling rates $\gamma = 0.05$ (top panel) and 0.01 (bottom panel), as a function of the scaled position $x = X/L$, for different system sizes $L = 1000$ (blue square), 2000 (magenta triangle) and 3000 (red circle) at hydrodynamic times $\tau = 0.1$ (for $\gamma = 0.05$) and 0.2 (for $\gamma = 0.01$), respectively. Throughout the analysis, we have done the averaging over 10^4 realizations. For both of these panels, we numerically integrate Eq. (6) with the already defined initial condition and the calculated $D_I(\rho, \gamma)$ for the respective parameter values, and the corresponding solution is plotted in black solid line. We observe the simulation points collapse onto each other and the curve for the collapsed data agrees very well with the analytic solution, thus immediately implying the existence of a diffusive scaling limit for model I.

V. SIMULATION RESULTS

A. Bulk-diffusion coefficients in models I and II

Using the methods mentioned in the previous section, we calculate the bulk-diffusion coefficient $D(\rho, \gamma)$ for both models in the parameter ranges $0.01 \leq \rho \leq 0.9$ and $0.001 \leq \gamma \leq 1$. For model II (LLG), we use the numerically obtained steady-state $P(g)$ in the analytic relation in Eq. (25), while for model I (standard RTPs), we follow the method described in Sec. IV B. In this section, we characterize the parameter dependence of $D(\rho, \gamma)$ in these two models. In Fig. 5a, we plot $D(\rho, \gamma)$, for model I, as a function of the tumbling rate γ at various densities $\rho = 0.01$ (blue square), 0.05 (red circle), 0.1 (black up triangle) and 0.5 (magenta down triangle). We observe the bulk-diffusion coefficient $D(\rho, \gamma)$ to be nonmonotonic in γ and the condition for optimized diffusion occurs when $\gamma \simeq \rho$. Notably, this is similar to the previous observations in Refs. [25, 31, 38] regarding the self-diffusivity of SPPs. Indeed, this nonmonotonic behavior clearly depicts the intriguing interplay of persistence and hard-core interaction in the system. In the case of $\gamma \gg \rho$, decreasing γ generates persistence to the particles, leading to the increment in $D(\rho, \gamma)$. However, in the other regime, i.e., $\gamma \ll \rho$, particles are *strongly interacting* and form jammed configuration. In this case, decreasing γ enhances the jamming condition further, resulting in the decrement in $D(\rho, \gamma)$. Moreover, we observe $D(\rho, \gamma) \sim \gamma$

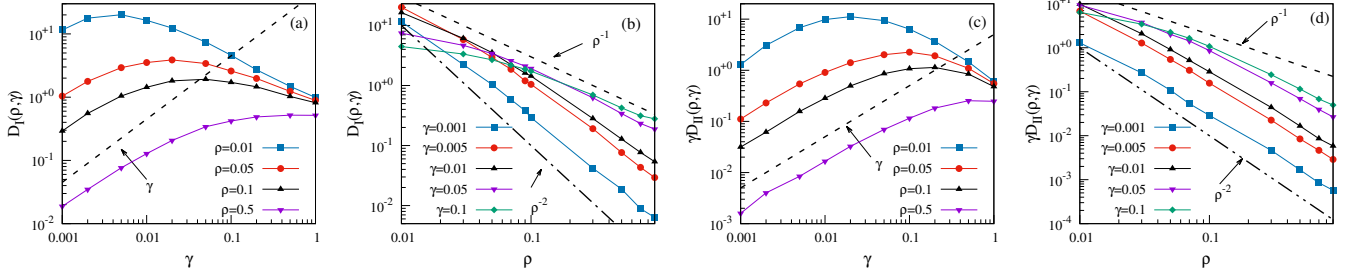


FIG. 5. *Bulk-diffusion coefficients in 1D.* We plot $D_I(\rho, \gamma)$ and $\gamma D_{II}(\rho, \gamma)$, as a function of γ at various densities $\rho = 0.01$ (blue square), 0.05 (red circle), 0.1 (black up triangle) and 0.5 (magenta down triangle) for model I [panel (a)] and model II [panel (c)], respectively. In panels (b) and (d), we plot $D_I(\rho, \gamma)$ and $\gamma D_{II}(\rho, \gamma)$, respectively as a function of ρ at various $\gamma = 0.001$ (blue square), 0.005 (red circle), 0.01 (black up triangle), 0.05 (magenta down triangle) and 0.1 (green diamond).

in this regime. This linear behavior in γ is quite expected, because diffusion occurs only when one of the boundary particles from a cluster flips, and the local spin-flipping event occurs at a time scale $\tau_p = 1/\gamma$, causing $D(\rho, \gamma)$ to scale as $1/\tau_p = \gamma$. In order to characterize the density dependence, in Fig. 5b, we plot $D(\rho, \gamma)$, for model I (standard RTPs), as a function of the density ρ at various tumbling rates $\gamma = 0.001$ (blue square), 0.005 (red circle), 0.01 (black up triangle), 0.05 (magenta down triangle) and 0.1 (green diamond). Unlike the previous case, here we find $D(\rho, \gamma)$ to decrease monotonically with ρ with a power-law tail, i.e., $D(\rho, \gamma) \sim \rho^{-\alpha}$, where the exponent α is parameter dependent. Quite interestingly, for model II (LLG), we observe $\gamma D(\rho, \gamma)$ to exhibit similar qualitative features. We show this by plotting $\gamma D(\rho, \gamma)$, for model II, as a function of γ and ρ in Figs. 5c and 5d, respectively, while keeping the other parameters same as model I.

Scaling collapse of the bulk-diffusion coefficient for small density and tumbling rate

We already observe that persistence and hard-core interaction compete with each other: While the former enhances diffusion, the latter diminishes it, resulting in non-monotonic variation of the bulk-diffusion coefficient as a function of tumbling rate, see Figs. 5a and 5c. Notably, we have analytically characterized this competing effect for model II via a scaling relation satisfied by $D(\rho, \gamma)$ in Eq. (33), and we have explicitly calculated the scaling function $\mathcal{F}(\psi)$ for 1D in Eq. (35). Here the scaling variable $\psi = \rho v/\gamma$ quantifies the intriguing interplay between persistence and interaction. Indeed, as in the model II, one can quantify this fascinating interplay using the same scaling variable ψ for the model I too. We verify these findings in Fig. 6.

In Figs. 6b and 6d, we plot $D_{II}(\rho, \gamma)/D_{II}^{(0)}$ as a function of ψ , for both 1D and 2D, respectively. Indeed we observe a nice scaling collapse and see an excellent agreement with $\mathcal{F}_{II}(\psi)$ for 1D as in Eq. (35), plotted in Fig. 6b (black solid line). For the model I, in Figs. 6a and 6c,

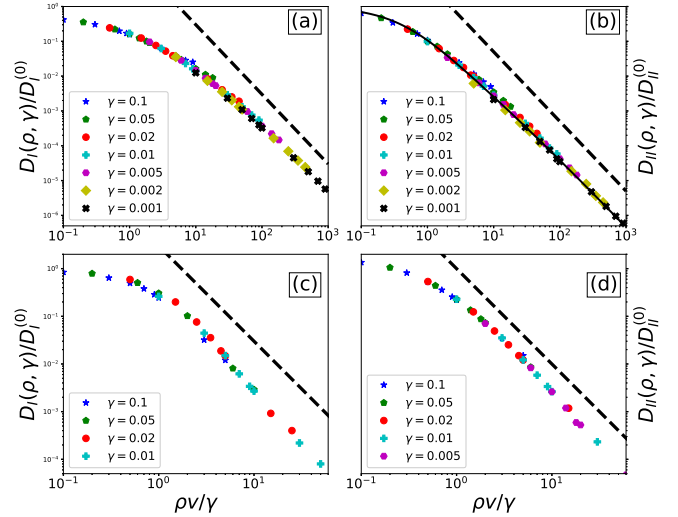


FIG. 6. *Scaling of the bulk-diffusion coefficient.* We plot scaled bulk-diffusion coefficients $D(\rho, \gamma)/D^{(0)}$ as a function of the scaled variable $\psi = \rho v/\gamma$ (with $v = 1$) for model I ((a) - 1D and (c) - 2D) and model II ((b) - 1D and (d) - 2D). The solid line in panel (b) represents the theory as in Eq. (35); the black dotted guiding lines represent $1/\psi^2$ behavior at large ψ .

we plot $D_I(\rho, \gamma)/D_I^{(0)} \equiv \mathcal{F}_I(\psi)$ as a function of ψ with $D_I^{(0)} = v^2/\gamma d$ for both 1D and 2D, respectively. We observe an excellent scaling collapse in both dimensions, confirming the existence of the scaling regime of $D(\rho, \gamma)$ for model I. Note that, the difference in the microscopic time unit in models I and II is reflected through the ratio $D_I^{(0)}/D_{II}^{(0)} = \gamma$. Moreover, as in the model II, we find that $\mathcal{F}_I(0) = \text{const.}$ and $\mathcal{F}_I(\psi) \simeq 1/\psi^2$ for $\psi \gg 1$. This reflects the fact that both model I and II have remarkably similar features, which is evident upon time rescaling for model I (standard RTPs): $\gamma t \rightarrow t$, with time measured in the unit of persistence time $\tau_p = \gamma^{-1}$.

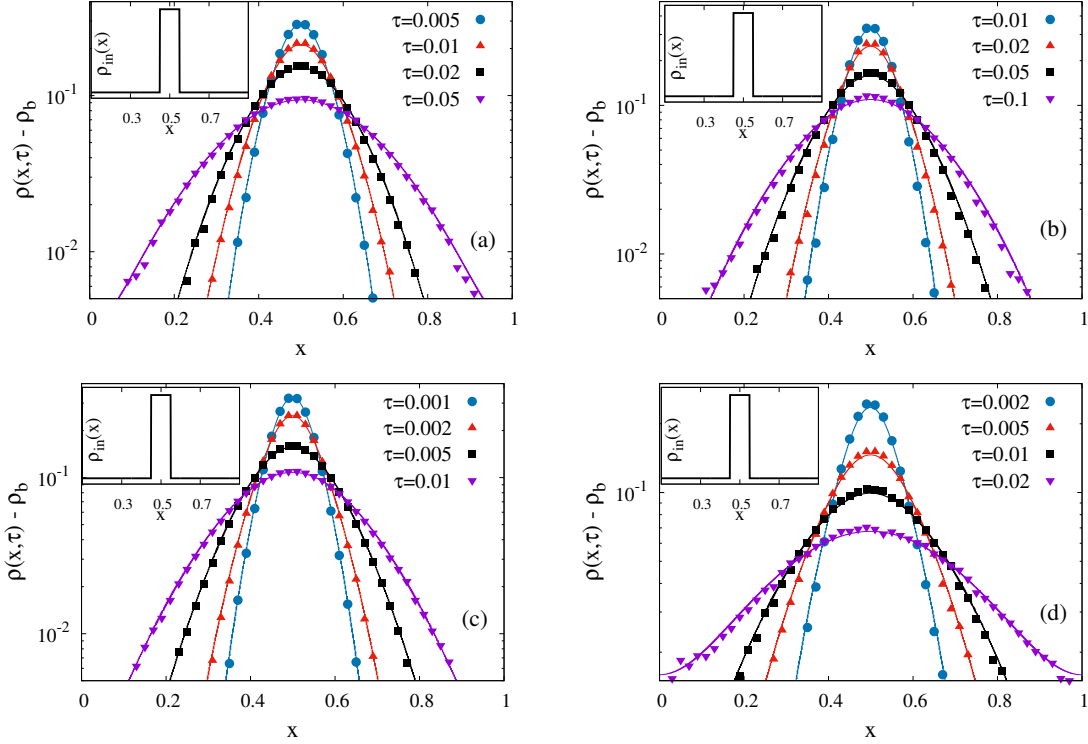


FIG. 7. *Verification of hydrodynamics at long-time.* We plot the numerically obtained excess density profile $\delta\rho(x, \tau) = \rho(x, \tau) - \rho_b$ for $\gamma = 0.05$ [model I (a) and model II (c)] and 0.01 [model I (b) and model II (d)] as a function of the scaled position x at various hydrodynamic time τ . In all of these panels, corresponding lines are obtained by integrating the hydrodynamic equation in Eq. (6) using same initial condition (shown in the inset) in Eq. (42) with $\rho_b = 0.5$, $\rho_1 = 0.4$ and $w = 0.1$.

B. Diffusive density relaxation

In this section, we verify the long time hydrodynamic description in $1D$, as shown in Eq. (6), by relaxing the initial density perturbation through the already obtained bulk-diffusion coefficients $D_I(\rho, \gamma)$ and $D_{II}(\rho, \gamma)$ for models I and II, respectively. For this purpose, we take the initial density perturbation $\rho_{in}(x) = \rho(x, 0)$ to be a step-function with step height ρ_1 and width w over a uniform background density ρ_b , which mathematically can be expressed as,

$$\rho_{in}(x) = \begin{cases} \rho_b + \rho_1 & \text{for } |x - \frac{1}{2}| \leq \frac{w}{2}, \\ \rho_b & \text{otherwise.} \end{cases} \quad (42)$$

We choose $\rho_1 = 0.4$, $\rho_b = 0.5$, $w = 0.1$ and $L = 1000$ for both the models. To verify Eq. (6), we plot the excess density $\delta\rho(x, \tau) = \rho(x, \tau) - \rho_b$ in Fig. 7, obtained from simulation (points), as a function of x at various times τ for $\gamma = 0.05$ [panel (a) for model I, panel (c) for model II] and 0.01 [panel (b) for model I, panel (d) for model II]. In order to obtain the theoretical predictions (line), we perform Euler integration of Eq. (6) by using the same initial condition and the already calculated bulk-diffusion coefficients [$D_I(\rho, \gamma)$ for model I and $D_{II}(\rho, \gamma)$ for model II]. For both γ , we find the hydrodynamic theory (line) remarkably captures the simulation data (points). Such

an agreement immediately verifies the bulk-diffusion coefficients and the existence of the hydrodynamic equation [i.e., Eq. (6)] for models I and II.

C. Emergent hydrodynamics

Although the obtained bulk-diffusion coefficients characterize the hydrodynamics quite well at the moderate persistence regime (see Sec. VB), $D_I(\rho, \gamma)$ shows anomalous behavior in the limit of strong persistence, i.e., $\gamma \rightarrow 0$; in the low density limit, it diverges as $1/\gamma$, while in the finite density limit, it vanishes as $D_I \sim \gamma$. Furthermore, on the time scale of RTPs, the bulk-diffusion coefficient of model II, i.e., $\gamma D_{II}(\rho, \gamma)$ exhibits similar characteristics. Consequently, the hydrodynamic description is not meaningful in the limit $\gamma \rightarrow 0$. Therefore, to maintain an appropriate hydrodynamic structure, one cannot independently vary ρ and γ and, from the scaling relation satisfied by $D(\rho, \gamma)$, we see that proper hydrodynamics scaling is recovered only when we rescale the density field $\psi = \rho/\gamma$ and time $\tilde{\tau} = \tau/\gamma$ (for model I) and $\tilde{\tau} = \tau/\gamma^2$ (for model II) and the corresponding hydrodynamic equation is given by,

$$\frac{\partial \psi(x, \tilde{\tau})}{\partial \tilde{\tau}} = \frac{\partial}{\partial x} \left[\mathcal{F}(\psi) \frac{\partial \psi(x, \tilde{\tau})}{\partial x} \right]. \quad (43)$$

To verify Eq. (43), in Fig. (8) we plot the scaled density field $\psi(x, \tilde{\tau}) = \rho(x, \tau = \tilde{\tau}\gamma)/\gamma$ for model I (standard RTPs) (top-panel) and $\rho(x, \tau = \tilde{\tau}\gamma^2)/\gamma$ for model II (bottom-panel) as a function of coarse-grained position $x = X/L$ for different γ and hydrodynamic time τ while keeping the rescaled time fixed at $\tilde{\tau} = \tau/\gamma$ and τ/γ^2 for models I and II, respectively. The hydrodynamic equation would be verified if different curves corresponding to different γ at the same $\tilde{\tau}$ collapse with each other and the collapsed profile at different $\tilde{\tau}$ is governed by the solution of Eq. (43). In order to verify this, we choose the initial scaled density profile $\psi_{in}(x) = \psi(x, \tilde{\tau} = 0)$ to be a step function with step height ψ_1 and width w over a uniform background profile ψ_b , i.e.

$$\psi_{in}(x) = \begin{cases} \psi_b + \psi_1 & \text{for } |x - \frac{1}{2}| \leq \frac{w}{2}, \\ \psi_b & \text{otherwise.} \end{cases} \quad (44)$$

For a fixed γ , we prepare a step profile for the density field $\rho(x, 0)$ with step height ρ_1 and width w around $x = 1/2$ over a uniform background density ρ_b such that the rescaled density $\psi_b = \rho_b/\gamma$ and $\psi_1 = \rho_1/\gamma$ remain fixed for all γ . In Fig. 8, for a fixed $\psi_b = 40$ and $\psi_1 = 40$, we plot the relaxation of the excess rescaled density $\psi(x, \tilde{\tau}) - \psi_b$, obtained from simulation, as a function of x for different $\gamma = 0.01$ (open symbols) and 0.005 (closed symbols) at various rescaled hydrodynamic time $\tilde{\tau} = 5, 10$ and 20 for model I (top-panel) and $\tilde{\tau} = 40, 80$ and 160 for model II (bottom-panel). In all of these panels, corresponding lines are obtained from numerical integration of Eq. (43) using $\mathcal{F}_I(\psi)$, obtained from simulation, for model I and $\mathcal{F}_{II}(\psi)$ for model II in Eq. (35). We observe, simulation data (points) and theory (lines) corresponding to these two different γ collapse quite well for both these models, which consequently verifies the existence of the proper hydrodynamic equation Eq. (43).

D. Anomalous transport

Finally, we analyze the issue of the anomalous time evolution of initially localized density profiles in these two models. We first rescale time for model I (standard RTPs) $\gamma t \rightarrow t$ (thus $D \rightarrow \gamma D$), putting the system on an equal footing with the model II (LLG). Now, at the onset of diffusion, i.e., at *early but long enough* time $1 \ll t \ll L^2/D$, particles have undergone many collisions and then local-density can safely be assumed to evolve through Eq. (5). Importantly, depending on density and persistence length, the bulk-diffusion coefficient can have a power-law dependence on density, i.e.,

$$D(\rho, \gamma) \simeq \frac{C}{\rho^\alpha}, \quad (45)$$

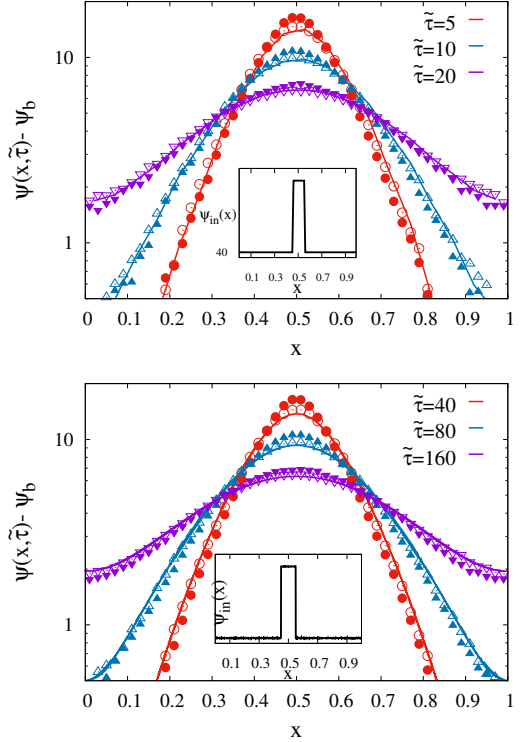


FIG. 8. *Verification of the emergent hydrodynamics.* We plot the scaled excess density field $\delta\psi(x, \tilde{\tau}) = \psi(x, \tilde{\tau}) - \psi_b$, for model I (top-panel) and model II (bottom-panel), as a function of the scaled position x at various rescaled time $\tilde{\tau}$ for two different $\gamma = 0.005$ (closed points) and 0.01 (open points). Corresponding lines are obtained by integrating Eq. (43) using the scaling function $\mathcal{F}_I(\psi)$ obtained from simulation and $\mathcal{F}_{II}(\psi)$ from Eq. (35). We observe a good collapse between simulation points and a reasonably good agreement with theory (lines).

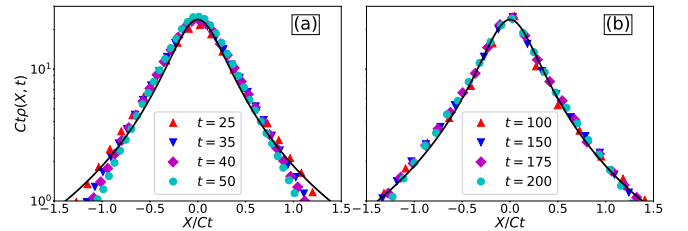


FIG. 9. *Anomalous transport.* We plot scaled density profile $Ct\rho(X, t)$ against scaled variable $\xi = X/Ct$ for model I (left panel) and model II (right panel). The spin-flipping rate $\gamma = 0.05$ ($l_p = 20$), $N = 20$ with $C = 3.2$ (for model I) and 2.2 (for model II); the black solid lines - the scaling solution $\mathcal{R}(\xi)$ in Eq. (49).

where the constant C and α ($0 \leq \alpha \leq 2$) depend on the parameter regime under consideration (see Sec. V A). Remarkably, for the above $D(\rho, \gamma)$ and *delta* initial condition $\rho(X, 0) = N\delta(X)$, Eq. (5) can be exactly solved

using the following scaling ansatz,

$$\rho(X, t) = \frac{1}{(Ct)^\omega} \mathcal{R}(\xi), \quad (46)$$

where $\xi = X/(Ct)^\omega$ is the scaling variable. Also, ω and $\mathcal{R}(\xi)$ are the growth exponent and the scaling function, which we will calculate in the subsequent section. Now, plugging the above scaling solution in Eq. (5) and transforming $X \rightarrow \xi = X/(Ct)^\omega$, we obtain the following evolution equation of $\mathcal{R}(\xi)$:

$$\omega \frac{d(\xi \mathcal{R})}{d\xi} = - (Ct)^{1-(2-\alpha)\omega} \frac{d}{d\xi} \left[\mathcal{R}^{-\alpha} \frac{d\mathcal{R}}{d\xi} \right]. \quad (47)$$

However, to exhibit self-similar solution, Eq. (47) should not contain t explicitly, implying $1 - (2 - \alpha)\omega = 0$, or

$$\omega = \frac{1}{2 - \alpha}. \quad (48)$$

Note that, Eq. (48) directly relates the growth exponent ω to the exponent α , which is a parameter dependent quantity. We now choose a parameter regime where $\alpha = 1$ and consequently $\omega = 1$ (thus the dynamic exponent $z = 1/\omega = 1$), implying a ballistic transport, quite strikingly within a framework of a diffusion equation (5), albeit a nonlinear one. By using conditions $\mathcal{R}(0) = 2/\xi_0^2$ and $\mathcal{R}'(0) = 0$, we exactly obtain,

$$\mathcal{R}(\xi) = \frac{2}{\xi_0^2 + \xi^2}, \quad (49)$$

with constant ξ_0 fixed through conservation condition $\int_{-\infty}^{\infty} \mathcal{R}(\xi) d\xi = \text{const.}$; in particular, for $\xi \gg 1$, $\mathcal{R}(\xi) \sim 1/\xi^2$ signifies a power-law decay. Thus the density relaxation has anomalous spatiotemporal scaling with a non-Gaussian spread, which however eventually becomes Gaussian (thus normal diffusion with $z = 2$). In simulation, we prepare the *delta*-like initial profile by considering the step initial condition in Eq. (42) in the narrow width limit, i.e., $w/L \ll 1$. In particular, the simulation parameters are following: $L = 1000$, $w = 20$, $\rho_0 = 0$, $\rho_1 = 1$, $\gamma = 0.05$. In Fig. 9, we plot the scaled density profile $Ct\rho(X, t)$ for model I (left) and II (right), obtained from simulation, as a function of X/Ct in the early-time regime; we have a nice scaling collapse and a reasonable agreement with theory (shown in solid black line); deviations at the tails are because the power-law behavior of $D(\rho, \gamma)$ is cut off at very low densities.

VI. SUMMARY

We study density relaxation in conventional models of interacting self-propelled particles (SPPs) in d dimensions on a periodic lattice of volume L^d for arbitrary density ρ and tumbling rate $\gamma = \tau_p^{-1}$. We consider a subclass of SPPs - two interacting models of run-and-tumble particles (RTPs): Model I is the standard version of hardcore RTPs introduced in Ref. [1], whereas model II is a

hardcore long-ranged lattice gas (LLG) - an analytically tractable variant of model I. Note that this particular class of RTPs considered here are unlike those studied in Ref. [25], where tumbling rate depends on system size and vanishes as $L \rightarrow \infty$; as a result, the large-scale evolution of the system is exactly described by mean-field hydrodynamics, which are obtained by calculating various averages, required to derive hydrodynamics, with respect to a product Bernoulli measure. On the other hand, the models considered in this paper have finite spatial correlations (which could be even long-ranged in the small tumbling-rate regime) and the nonequilibrium steady-state measure is not known.

In the above mentioned models I and II, we characterize collective diffusion (i.e., density relaxations), caused by subtle many-body effects arising from an intriguing interplay between interaction and persistence, through precise quantitative determination of the density- and tumbling-rate-dependent bulk-diffusion coefficient. We scale original position \mathbf{X} and time t as $\mathbf{x} = \mathbf{X}/L$ and time $\tau = t/L^2$ take the thermodynamic limit (system size $L \rightarrow \infty$ and particle number $N \rightarrow \infty$ with global density N/L^d fixed). We then show that the hydrodynamic density field $\rho(\mathbf{x}, \tau)$ satisfies a nonlinear diffusion equation $\partial_\tau \rho(\mathbf{x}, \tau) = \nabla[D(\rho, \gamma)\nabla\rho(\mathbf{x}, \tau)]$, where $D(\rho, \gamma)$ is the bulk-diffusion coefficient, which, we show, has a power-law form, i.e., $D \sim \rho^{-\alpha}$ with $0 < \alpha \leq 2$ in broad range of parameter values. We calculate the bulk-diffusion coefficient as a function of density and tumbling rate (i) analytically for model II (LLG version) and (ii) numerically in model I (standard hardcore RTPs) through an efficient Monte Carlo simulation algorithm; we also verify the analytical results for model II in simulations.

Remarkably, the many-body correlations in these models manifest themselves through anomalous transport and emerge through the competition between two length scales - the ‘‘mean free path’’ and the persistence length. Indeed, local structural relaxations are sensitive to local densities and produce a wide range of time scales (power-law distributed), thus resulting in dynamical heterogeneity and anomalous transport. In particular, we also investigate the most interesting case when tumbling rate becomes small. In the limit of $\rho \rightarrow 0$ and $\gamma \rightarrow 0$ with the ratio ρ/γ fixed, the bulk-diffusion coefficient satisfies a scaling law $D(\rho, \gamma) = D^{(0)}\mathcal{F}(\rho/\gamma)$ of Eq. (2). Furthermore, for model II in one dimension, we analytically calculate the scaling function $\mathcal{F}(\psi)$, which is in excellent agreement with simulations. Our findings, as succinctly expressed in Eq. (2), are of particular significance: They are independent of dimensions and microscopic details and unveil a unique mechanism of collective transport - *diffusive, yet anomalous* - that has not been identified previously in SPPs. However, the exact functional form of $\mathcal{F}(\psi)$ depends on microscopic details.

Notably, the order of hydrodynamic limits is important. When the large persistence-time limit is taken first, followed by the large system-size limit, the system undergoes a previously studied ‘‘jamming’’ or dynamical ar-

rest [66]. On the other hand, studies in Refs. [25, 29] considered system-size dependent tumbling rate, which, though, differs from the standard versions of SPPs - the main motivation behind our work [1, 31, 57, 58, 67, 68]. In our study, the large system-size limit is taken first, followed by the large persistence-time limit. Indeed, attempts to develop a rigorous hydrodynamic description of SPPs that correspond to this specific order of limit have not been successful so far. Recently, the bulk-diffusion coefficient for a dual version of hardcore RTPs in the leading order of tumbling rate has been calculated [69] and it agrees well with Eq. (2) as $\psi \rightarrow \infty$. However, none of these previous works realized the existence of a generic scaling regime for bulk diffusion, which we identify here. Interestingly, in a different context, a similar scaling regime for the self-diffusion coefficient in variants of SPPs has recently been observed in Ref. [36], which

nicely complements our findings. However, the precise relationship between the bulk- and self-diffusion coefficients currently remains unclear. In this scenario, our proposed mechanism of density relaxations could provide useful insights into collective transport in SPPs and will open up new research avenues.

ACKNOWLEDGMENTS

We thank Subhadip Chakraborti, Arghya Das, Rahul Dandekar and R. Rajesh for discussions. P.P. gratefully acknowledges the Science and Engineering Research Board (SERB), India, under Grant No. MTR/2019/000386, for financial support. T.C. acknowledges a research fellowship [Grant No. 09/575 (0124)/2019-EMRI] from the Council of Scientific and Industrial Research (CSIR), India.

APPENDIX

In the appendix section, we provide additional calculation and derivation details, as well as simulation results used in the main text.

A. Verification of the scaling form of gap distribution $P(g)$

In this section, we numerically verify the scaling relation satisfied by the typical gap size g_* in the regime of low density and strong persistence used in the main text in Eq. (30), i.e.,

$$g_* = \frac{1}{\rho} \mathcal{G}(\psi). \quad (50)$$

Note that, using the assumed exponential form of the gap distribution, i.e.,

$$P(g) \simeq N_* e^{-g/g_*} \quad (51)$$

and the above scaling form of g_* in the following conservation equation

$$\langle g \rangle = \sum_{g=1}^{\infty} g P(g) = 1/\rho, \quad (52)$$

which is exact in the low density limit, we straightforwardly obtain the proportionality constant

$$N_* = \frac{1}{\rho} \frac{[\exp(\rho/\mathcal{G}(\psi)) - 1]^2}{\exp(\rho/\mathcal{G}(\psi))}. \quad (53)$$

Now, inserting g_* and N_* , as shown in Eqs. (50) and (53), in the expression of $P(g)$ in Eq. (51), we obtain the following scaling relation for $P(g)$,

$$-\ln \left(\frac{P(g)}{\rho} \right) = \frac{\rho g}{\mathcal{G}(\psi)} + 2 \ln(\mathcal{G}(\psi)). \quad (54)$$

Clearly, the above scaling relation is a direct consequence of the assumed scaling form of g_* in Eq. (50). Hence, verifying Eq. (54) yields the existence of the proposed scaling relation of g_* right away. In order to do so, we compute and plot the steady-state $P(g)$ for model I (left panel) and model II (right panel) in 1D at various tumbling rates

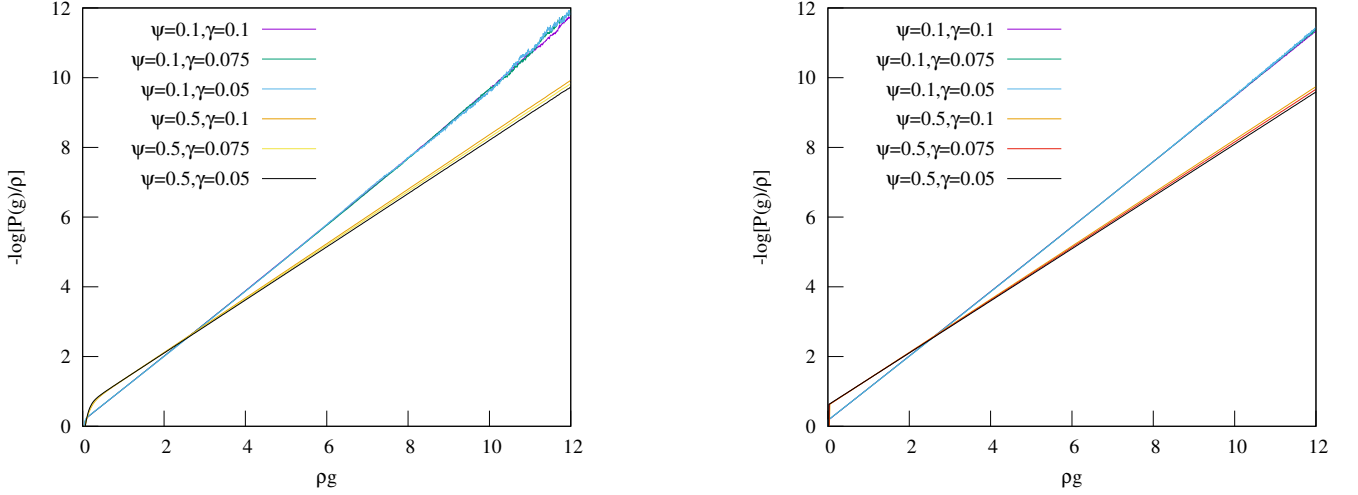


FIG. 10. *Verification of Eq. (54)*. We plot $-\ln(P(g)/\rho)$ as a function of ρg for model I (left-panel) and model II (right-panel) in $1D$, for various combinations of ρ and γ such that the scaling variable ψ remains fixed at 0.1 and 0.5. In both these panels, for $\psi = 0.1$, we have used $\gamma = 0.1$ (magenta line), 0.05 (green line) and 0.01 (sky blue line); while the same for $\psi = 0.5$ are shown in orange line, black line and blue line respectively.

γ (various persistent length for model II) and densities ρ , while keeping the ratio $\psi = \rho v/\gamma$ constant. The scaling relation would be verified if data points corresponding to different ρ and γ at a fixed ψ collapse with each other.

To check this, in Fig. 10, we plot $-\ln(P(g)/\rho)$ as a function of the scaled gap size ρg for model I (left) and model II (right) at two different $\psi = 0.1$ and 0.5. For each ψ , we have used three different tumbling rates $\gamma = 0.05, 0.075$, and 0.1 and the corresponding density ρ is chosen from the relation $\rho = \gamma\psi/v$ (where $v = 1$). Data belonging to different parameter spaces (ρ, γ) corresponding to the same ψ collapse quite well, as shown in the figure. This observation immediately validates the scaling form of g_* for both models I and II.

B. Derivation of scaling function $\mathcal{F}_{II}(\psi)$ of the bulk-diffusion coefficient in model II

In this section, we derive the analytic expressions for the bulk-diffusion coefficient $D_{II}(\rho, \gamma)$ and the corresponding scaling function $\mathcal{F}_{II}(\psi)$, presented in the main text in Eq. (34). Using the gap distribution function given in Eq. (51) in the calculated expression of the bulk-diffusion coefficient $D_{II}(\rho, \gamma)$, shown in the main text in Eq (25), we obtain,

$$D_{II}(\rho, \gamma) = -\frac{1}{2d} \frac{\partial}{\partial \rho} \left[N_* \rho \sum_{l=1}^{\infty} \phi(l) \left(\sum_{g=1}^{\infty} g e^{-g/g_*} + (l-1) \sum_{g=l}^{\infty} (g-l) e^{-g/g_*} \right) \right]. \quad (55)$$

We now note the following identities:

$$\sum_{g=1}^{\infty} g e^{-g/g_*} = \langle g \rangle, \quad (56)$$

$$\sum_{g=l}^{\infty} (g-l) e^{-g/g_*} = e^{-l/g_*} \frac{\langle g \rangle}{N_*}, \quad (57)$$

$$\langle g \rangle = \frac{1}{\rho} - 1. \quad (58)$$

Here $\langle g \rangle$ is the mean gap length at density ρ . Now, using these identities and $\phi(l) = B e^{-l/l_p}$ in Eq. (55), we obtain

$$D_{II}(\rho, \gamma) = -\frac{B}{2d} \frac{\partial}{\partial \rho} \left[(1-\rho) \left\{ \sum_{l=1}^{\infty} e^{-l/l_p} + \sum_{l=1}^{\infty} (l-1) e^{-l/\xi} \right\} \right], \quad (59)$$

where we define $\xi = 1/(1/l_p + 1/g_*)$. It is now easy to perform the summations appearing in Eq. (59), which are given by,

$$\sum_{l=1}^{\infty} e^{-l/l_p} = \frac{1}{e^{1/l_p} - 1}, \quad (60)$$

$$\sum_{l=1}^{\infty} (l-1)e^{-l/\xi} = \frac{1}{(e^{1/\xi} - 1)^2}. \quad (61)$$

Finally, replacing Eqs. (60) and (62) in Eq. (59), we obtain the following simplified form:

$$D_{II}(\rho, \gamma) = -\frac{B}{2d} \frac{\partial}{\partial \rho} \left[(1-\rho) \left\{ \frac{1}{e^{1/l_p} - 1} + \frac{1}{(e^{1/\xi} - 1)^2} \right\} \right]. \quad (62)$$

Notably, the above form of $D_{II}(\rho, \gamma)$ is used in the main text in Eq. (26) and is valid for arbitrary values of ρ and γ . However, in the subsequent analysis, we consider the following special cases:

- Case I, ρ arbitrary, $\gamma \rightarrow \infty$: In this case, we have $B = 1$ and the typical gap size g_* is given by,

$$g_* = -\frac{1}{\log(1-\rho)}. \quad (63)$$

Using this particular g_* and $\gamma \rightarrow \infty$ or $l_p \rightarrow 0$ in Eq. (62), it is straightforward to show that the second term in the curly bracket does not contribute, and the resulting expression of $D_{II}(\rho, \gamma)$ is given by,

$$D_{II}(\rho, \gamma) = e^{-1/l_p} D_{SSEP}, \quad (64)$$

where $D_{SSEP} = 1/2d$ is the bulk-diffusion coefficient for SSEP in d dimension.

- Case II, ρ finite and large, $\gamma \rightarrow 0$: In this case, we have $B = 1/l_p$ and the typical gap size, as calculated in Ref. [63], is given by

$$g_* = \sqrt{l_p \langle g \rangle}, \quad (65)$$

which immediately implies,

$$\frac{\partial g_*}{\partial \rho} = -\frac{1}{2\rho^2} \sqrt{\frac{l_p}{\langle g \rangle}}. \quad (66)$$

Moreover, using the g_* mentioned above, we obtain

$$\xi = \frac{l_p}{1 + \sqrt{\frac{l_p}{\langle g \rangle}}}. \quad (67)$$

Notably, in this regime, l_p , g_* and ξ are infinitely large. Using all of the above relations in Eq. (62) and after some algebraic manipulations, we finally obtain a simplified expression of $D(\rho, \gamma)$ in this regime, which is given by,

$$D_{II}(\rho, \gamma) = \frac{1}{2\rho^2}. \quad (68)$$

- Case III, $\rho \rightarrow 0$, $\gamma \rightarrow 0$: In this particular regime of interest, the typical gap size g_* obeys the following scaling relation:

$$g_* = \frac{1}{\rho} \mathcal{G}(\psi), \quad (69)$$

where $\psi = \rho/\gamma$. Using the above expression of g_* , we can easily calculate

$$\frac{\partial g_*}{\partial \rho} = -\frac{g_*}{\rho} \left(1 - \psi \frac{\mathcal{G}'(\psi)}{\mathcal{G}(\psi)} \right). \quad (70)$$

Note that, since $\rho \rightarrow 0$, we can easily write $1 - \rho \simeq 1$, which simplifies Eq. (62) substantially. Finally, substituting all of the results in Eq. (62), some algebraic manipulations leads to the following expression of the bulk-diffusion coefficient:

$$D_{II}(\rho, \gamma) = \frac{e^{1/\xi}}{l_p d (e^{1/\xi} - 1)^3} \frac{1}{\mathcal{G}(\psi)} \left(1 - \psi \frac{\mathcal{G}'(\psi)}{\mathcal{G}(\psi)} \right). \quad (71)$$

Asymptotic expansion of $D_{II}(\rho, \gamma)$: We further expand the bulk-diffusion coefficient $D_{II}(\rho, \gamma)$, obtained in Eq. (71), in the limit of $\gamma \rightarrow 0$ and $\rho \rightarrow 0$, such that the dimensionless quantity $\psi = \rho v / \gamma$ remains finite. Let us first make the replacement,

$$\frac{1}{\xi} = n = \frac{1}{l_p} + \frac{\rho}{\mathcal{G}(\psi)} = \frac{1}{l_p} \left(1 + \frac{\psi}{\mathcal{G}(\psi)} \right). \quad (72)$$

Note that this particular limit of interest automatically implies $n \rightarrow 0$. We now expand the following expression as

$$\begin{aligned} \frac{e^n}{l_p (e^n - 1)^3} &= \frac{\left(1 + n + \frac{n^2}{2} \dots \right)}{l_p n^3 \left(1 + \frac{n}{2} + \frac{n^2}{6} \dots \right)^3} \\ &\simeq \frac{1}{l_p} \left(\frac{1}{n^3} - \frac{1}{2n^2} - \frac{3}{2n} \dots \right). \end{aligned} \quad (73)$$

Since we are working in the regime $n \rightarrow 0$, the leading order contribution to Eq. (73) emerges from $1/n^3$ term only and consequently the bulk-diffusion coefficient can be written as

$$\begin{aligned} D_{II}(\rho, \gamma) &= \frac{1}{l_p d n^3 \mathcal{G}(\psi)} \left(1 - \psi \frac{\mathcal{G}'(\psi)}{\mathcal{G}(\psi)} \right) + \mathcal{O} \left(\frac{\gamma}{n^2} \right), \\ &\simeq \frac{l_p^2 \mathcal{G}^2(\psi)}{d (\mathcal{G}(\psi) + \psi)^3} \left(1 - \psi \frac{\mathcal{G}'(\psi)}{\mathcal{G}(\psi)} \right) + \mathcal{O}(l_p). \end{aligned} \quad (74)$$

From the above equation, it is quite evident that $D_{II}(\rho, \gamma)$ satisfies a scaling relation and the corresponding scaling function can be written as

$$\mathcal{F}_{II}(\rho, \gamma) = \frac{1}{d} \left(\frac{\gamma}{v} \right)^2 D_{II}(\rho, \gamma) \simeq \frac{\mathcal{G}^2(\psi)}{(\mathcal{G}(\psi) + \psi)^3} \left(1 - \psi \frac{\mathcal{G}'(\psi)}{\mathcal{G}(\psi)} \right), \quad (75)$$

which we have used in the main text in Eq. (34).

-
- [1] R. Soto and R. Golestanian, Phys. Rev. E **89**, 012706 (2014).
 - [2] M. C. Marchetti, J. F. Joanny, S. Ramaswamy, T. B. Liverpool, J. Prost, M. Rao, and R. A. Simha, Rev. Mod. Phys. **85**, 1143 (2013).
 - [3] X.-L. Wu and A. Libchaber, Phys. Rev. Lett. **84**, 3017 (2000).
 - [4] B. Wang, S. M. Anthony, S. C. Bae, and S. Granick, Proceedings of the National Academy of Sciences **106**, 15160 (2009), <https://www.pnas.org/doi/pdf/10.1073/pnas.0903554106>.
 - [5] K. C. Leptos, J. S. Guasto, J. P. Gollub, A. I. Pesci, and R. E. Goldstein, Phys. Rev. Lett. **103**, 198103 (2009).
 - [6] A. Kudrolli, Phys. Rev. Lett. **104**, 088001 (2010).
 - [7] B. Wang, J. Kuo, S. C. Bae, and S. Granick, Nature Materials **11**, 481 (2012).
 - [8] G. Ariel, A. Rabani, S. Benisty, J. D. Partridge, R. M. Harshey, and A. Be'Er, Nature communications **6**, 1 (2015).
 - [9] H. M. López, J. Gachelin, C. Douarche, H. Auradou, and E. Clément, Phys. Rev. Lett. **115**, 028301 (2015).
 - [10] A. Cavagna, D. Conti, C. Creato, L. Del Castello, I. Giardina, T. S. Grigera, S. Melillo, L. Parisi, and M. Viale, Nature Physics **13**, 914 (2017).
 - [11] A. Sokolov, L. D. Rubio, J. F. Brady, and I. S. Aranson, Nature communications **9**, 1 (2018).
 - [12] A. G. Cherstvy, O. Nagel, C. Beta, and R. Metzler, Physical Chemistry Chemical Physics **20**, 23034 (2018).

- [13] A. Lagarde, N. Dagès, T. Nemoto, V. Démery, D. Bartolo, and T. Gibaud, *Soft Matter* **16**, 7503 (2020).
- [14] P. T. Underhill, J. P. Hernandez-Ortiz, and M. D. Graham, *Phys. Rev. Lett.* **100**, 248101 (2008).
- [15] Z. Liao, M. Han, M. Fruchart, V. Vitelli, and S. Vaikuntanathan, *The Journal of chemical physics* **151**, 194108 (2019).
- [16] D. Breoni, M. Schmiedeberg, and H. Löwen, *Phys. Rev. E* **102**, 062604 (2020).
- [17] Y. Hatwalne, S. Ramaswamy, M. Rao, and R. A. Simha, *Phys. Rev. Lett.* **92**, 118101 (2004).
- [18] S. Belan and M. Kardar, *The Journal of Chemical Physics* **150**, 064907 (2019).
- [19] A. R. Dulaney and J. F. Brady, *Phys. Rev. E* **101**, 052609 (2020).
- [20] P. Le Doussal, S. N. Majumdar, and G. Schehr, *EPL (Europhysics Letters)* **130**, 40002 (2020).
- [21] S. C. Takatori, R. De Dier, J. Vermant, and J. F. Brady, *Nature communications* **7**, 1 (2016).
- [22] P. Dolai, A. Das, A. Kundu, C. Dasgupta, A. Dhar, and K. V. Kumar, *Soft Matter* **16**, 7077 (2020).
- [23] F. Peruani, J. Starruß, V. Jakovljevic, L. Søgaard-Andersen, A. Deutsch, and M. Bär, *Phys. Rev. Lett.* **108**, 098102 (2012).
- [24] A. B. Slowman, M. R. Evans, and R. A. Blythe, *Phys. Rev. Lett.* **116**, 218101 (2016).
- [25] M. Kourbane-Houssene, C. Erignoux, T. Bodineau, and J. Tailleur, *Phys. Rev. Lett.* **120**, 268003 (2018).
- [26] S. Dal Cengio, D. Levis, and I. Pagonabarraga, *Phys. Rev. Lett.* **123**, 238003 (2019).
- [27] M. J. Metson, M. R. Evans, and R. A. Blythe, *Journal of Statistical Mechanics: Theory and Experiment* **2020**, 103207 (2020).
- [28] X.-q. Shi, G. Fausti, H. Chaté, C. Nardini, and A. Solon, *Phys. Rev. Lett.* **125**, 168001 (2020).
- [29] T. Agranov, S. Ro, Y. Kafri, and V. Lecomte, *Journal of Statistical Mechanics: Theory and Experiment* **2021**, 083208 (2021).
- [30] O. Chepizhko and F. Peruani, *Phys. Rev. Lett.* **111**, 160604 (2013).
- [31] D. Levis and L. Berthier, *Phys. Rev. E* **89**, 062301 (2014).
- [32] A. Liliushvili, J. Ónody, and T. Voigtmann, *Phys. Rev. E* **96**, 062608 (2017).
- [33] T. Bertrand, Y. Zhao, O. Bénichou, J. Tailleur, and R. Voituriez, *Phys. Rev. Lett.* **120**, 198103 (2018).
- [34] S. Put, J. Bex, and C. Vanderzande, *Journal of Statistical Mechanics: Theory and Experiment* **2019**, 123205 (2019).
- [35] P. Singh and A. Kundu, *Journal of Physics A: Mathematical and Theoretical* **54**, 305001 (2021).
- [36] V. E. Debets, X. M. de Wit, and L. M. C. Janssen, *Phys. Rev. Lett.* **127**, 278002 (2021).
- [37] P. Rizkallah, A. Sarracino, O. Bénichou, and P. Illien, *Phys. Rev. Lett.* **128**, 038001 (2022).
- [38] O. Granek, Y. Kafri, and J. Tailleur, *Physical Review Letters* **129**, 038001 (2022).
- [39] C. Kurzthaler, C. Devailly, J. Arlt, T. Franosch, W. C. K. Poon, V. A. Martinez, and A. T. Brown, *Phys. Rev. Lett.* **121**, 078001 (2018).
- [40] E. Irani, Z. Mokhtari, and A. Zippelius, *Phys. Rev. Lett.* **128**, 144501 (2022).
- [41] T. Arnoult de Pirey, G. Lozano, and F. van Wijland, *Phys. Rev. Lett.* **123**, 260602 (2019).
- [42] S. C. Takatori, W. Yan, and J. F. Brady, *Phys. Rev. Lett.* **113**, 028103 (2014).
- [43] A. P. Solon, J. Stenhammar, R. Wittkowski, M. Kardar, Y. Kafri, M. E. Cates, and J. Tailleur, *Phys. Rev. Lett.* **114**, 198301 (2015).
- [44] A. K. Omar, H. Row, S. A. Mallory, and J. F. Brady, *Proceedings of the National Academy of Sciences* **120**, e2219900120 (2023).
- [45] T. Speck, *Physical Review E* **103**, 012607 (2021).
- [46] S. Chakraborti, S. Mishra, and P. Pradhan, *Phys. Rev. E* **93**, 052606 (2016).
- [47] T. Chakraborty and P. Pradhan, (2023), arXiv:2309.02896 [cond-mat.stat-mech].
- [48] T. Bodineau and B. Derrida, *Physical review letters* **92**, 180601 (2004).
- [49] L. Bertini, A. De Sole, D. Gabrielli, G. Jona-Lasinio, and C. Landim, *Physical Review Letters* **87**, 040601 (2001).
- [50] C. Kipnis and C. Landim, *Scaling limits of interacting particle systems*, Vol. 320 (Springer Science & Business Media, 1998).
- [51] H. Spohn, *Large scale dynamics of interacting particles* (Springer Science & Business Media, 2012).
- [52] C. Arita, P. L. Krapivsky, and K. Mallick, *Phys. Rev. E* **90**, 052108 (2014).
- [53] J. M. Carlson, E. R. Grannan, and G. H. Swindle, *Phys. Rev. E* **47**, 93 (1993).
- [54] K. Malakar, V. Jemseena, A. Kundu, K. V. Kumar, S. Sabhapandit, S. N. Majumdar, S. Redner, and A. Dhar, *Journal of Statistical Mechanics: Theory and Experiment* **2018**, 043215 (2018).
- [55] A. Slowman, M. Evans, and R. Blythe, *Journal of Physics A: Mathematical and Theoretical* **50**, 375601 (2017).
- [56] A. Das, A. Dhar, and A. Kundu, *Journal of Physics A: Mathematical and Theoretical* **53**, 345003 (2020).
- [57] Y. Fily and M. C. Marchetti, *Phys. Rev. Lett.* **108**, 235702 (2012).
- [58] G. S. Redner, M. F. Hagan, and A. Baskaran, *Phys. Rev. Lett.* **110**, 055701 (2013).
- [59] J. Bialké, H. Löwen, and T. Speck, *Europhysics Letters* **103**, 30008 (2013).
- [60] M. J. Schnitzer, *Phys. Rev. E* **48**, 2553 (1993).
- [61] G. H. Weiss, *Physica A: Statistical Mechanics and its Applications* **311**, 381 (2002).
- [62] T. Chakraborty, S. Chakraborti, A. Das, and P. Pradhan, *Phys. Rev. E* **101**, 052611 (2020).
- [63] S. Chakraborti, T. Chakraborty, A. Das, R. Dandekar, and P. Pradhan, *Phys. Rev. E* **103**, 042133 (2021).
- [64] In the limit $\psi \rightarrow 0$ ($\rho \ll \gamma$), the dynamics in fact reduces to the well known simple symmetric exclusion process (SSEP), in which case $P(g) \sim (1 - \rho)^g$ and the corresponding typical gap size is given by $g_* = -1/\ln(1 - \rho) \simeq 1/\rho$, which is the average interparticle spacing..
- [65] S. Katz, J. L. Lebowitz, and H. Spohn, *Journal of statistical physics* **34**, 497 (1984).
- [66] R. Mandal, P. J. Bhuyan, P. Chaudhuri, C. Dasgupta, and M. Rao, *Nature communications* **11**, 2581 (2020).
- [67] G. Szamel, *Physical Review E* **90**, 012111 (2014).
- [68] C. Maggi, U. M. B. Marconi, N. Gnan, and R. Di Leonardo, *Scientific reports* **5**, 1 (2015).
- [69] R. Dandekar, S. Chakraborti, and R. Rajesh, *Phys. Rev. E* **102**, 062111 (2020).